J. Fluid Mech. (1993), *vol.* 253, *pp.* 297–326

Axisymmetric magnetoconvection in a twisted field

By C. A. JONES[1] AND D. J. GALLOWAY[2]

[1] Department of Mathematics, University of Exeter EX4 4QE, UK

[2] School of Mathematics and Statistics, University of Sydney, NSW 2006, Australia

(Received 20 August 1992 and in revised form 10 February 1993)

The process of flux rope formation in a convecting cell is studied. The magnetic field has both a meridional and an azimuthal component, and so corresponds to a twisted field. Convection occurs in this cylindrical cell because of heating from below, and is assumed to take an axisymmetric form. Only the Boussinesq problem is studied here, but both the kinematic and the dynamic regimes are considered.

The two cases where the twisted field is due to (*a*) an imposed flux of vertical current and (*b*) an imposed flux of vertical vorticity are considered. Strongly twisted ropes can be generated more easily in case (*b*) than in case (*a*).

We show that convection can produce ropes twisted in the opposite direction from that of the initial field. We also find that solutions can be oscillatory even when linear theory predicts steady solutions.

1. Introduction

There is now abundant evidence that the solar magnetic field is concentrated into ropes of magnetic flux (see e.g. Priest 1982). A key process for this concentration is the interaction between the magnetic field and convection taking place on and below the photosphere of the Sun. Convective eddies shepherd flux into comparatively stagnant regions at the cell boundaries, or, in axisymmetric flows, at the cell centre. A simple configuration in which this process can be analysed is an axisymmetric convecting cell, with gravity parallel to the cylinder axis, and an unstable temperature gradient. A magnetic field with an initially uniform vertical component is applied across the cylinder. The case where the magnetic field has no azimuthal component was examined by Galloway, Proctor & Weiss (1978), and Galloway & Moore (1979). For reviews of this and related work, see Proctor & Weiss (1982), Hughes & Proctor (1988), or see Nordlund *et al.* (1992) for a complementary approach where an ambitious large-scale simulation is described.

The new situation analysed in this paper is the case when there is an azimuthal as well as an axial magnetic field. This corresponds to a twisted field, which implies the existence of axial (and radial) currents flowing in the cylinder. In this situation, Lorentz forces will drive an azimuthal swirl around the cylinder, which can in turn affect the magnetic field. This work is partly motivated by the desire to understand the process of flux concentration at supergranule boundaries: the observed field structure is often considerably more complex than the twist-free field assumed by the standard theory. We are also interested in assessing the extent to which convection cells which happen to have substantial helical motions can twist up magnetic field, thereby generating vertical currents. On the Sun, such currents would pass up into the overlying chromosphere and corona, giving the field there the non-potential character it needs to be able to produce various forms of solar activity, as well as coronal heating. A

discussion of observations of these currents is given in Melrose (1991), together with an analysis of the theoretical problems they pose.

The development of convection in the presence of twisted fields is also of importance in planetary interiors: however, in this application rapid rotation is often important, whereas this is not the case in the present work. Nevertheless, we explore values of the Roberts number $q = \kappa/\eta$ which are both greater than unity (the most common case in stars), and less than unity (appropriate for planetary interiors). We recall that at $q > 1$ magnetoconvection with a purely axial field can occur in oscillatory form if the Chandrasekhar number Q is large enough. As we shall see, in this problem oscillatory behaviour can occur at both $q > 1$ and $q < 1$; also, if the curved boundary of the cell is rotating, it is possible for oscillations to occur even at small Chandrasekhar number.

The present work makes two substantial simplifications over the astrophysical problem right at the outset: our study is Boussinesq (i.e. almost incompressible), and only axisymmetric solutions are considered. The use of the Boussinesq assumption has been well-documented (Proctor & Weiss 1982), and whilst care is obviously necessary in applying the results, more involved compressible calculations have confirmed the general picture provided by Boussinesq models of magnetoconvection. The assumption of axisymmetry is more problematic. Particularly for large twists, the whole zoo of plasma pinch instabilities can enter the picture, and in many cases it is known that non-axisymmetric modes are the most unstable. We have attempted to show in §3 that it is at least plausible that there are parameter regimes where axisymmetric modes are preferred, and we expect convection may reinforce this tendency. Examples of axisymmetric twisted sunspots on the Sun show that such configurations can and do exist in Nature. But our main reason for assuming axisymmetry is to keep the problem manageable, both computationally and from the point of view of theoretical understanding. Even so, the results are complicated, and sensitive to the way the problem is driven through the boundary conditions.

Some progress was made on this problem by Childress (1979), using asymptotic methods. The main focus of attention there was the calculation of the strength of the dynamo-theoretic α-effect, which is non-zero in this geometry because of the non-zero helicity. This was subsequently extended to the context of fast dynamos by Childress & Soward (1985) and Soward & Childress (1986). We have related our model to this work elsewhere (Jones & Galloway 1993), showing in particular how the α-effect is suppressed when the central magnetic flux rope becomes dynamically active. In this paper we concentrate on more basic issues such as the formation of twisted flux ropes, the distribution of angular momentum, and the appearance of steady or oscillatory convection.

There are a number of different ways in which an azimuthal field can be created (we are not here considering a dynamo, so that azimuthal field will decay unless it is imposed somehow from the boundary, or driven by differential rotation). Here these are represented by applying different boundary conditions. The conditions we will consider fall into two classes, those in which a vertical current passes through the endwalls of the cell, and those in which the curved boundary is rotated at a certain angular velocity.

The first situation could arise when an initially untwisted flux tube of uniform field strength is given a twist through a finite angle, which creates a uniform vertical current. Then convection occurs, and concentration of the twisted flux tube takes place. The convective part of this process can be modelled by specifying B_ϕ on the curved boundary, which ensures that the integrated vertical current through the cylinder is

fixed. Even within this model we can vary the boundary conditions on the azimuthal velocity, and two possibilities are considered.

The second situation occurs when the integrated flux of vertical vorticity through the cell is prescribed, rather than the current. This implies that the angular velocity on the curved boundary is fixed. This then generates azimuthal field through differential rotation. In stars, such rotational driving is to be expected on the largest scales by virtue of the Coriolis force. For the smaller scales occurring at supergranule boundaries (where our model is at its most appropriate), the cells may be embedded in a region of non-zero vorticity having its origin in the solar rotation and being enhanced by the large-scale motion. It is in the nature of turbulence that convecting eddies will sometimes have net rotation even on small scales, although how persistent this will be is unclear.

Section 2 sets up the problem in terms of equations and boundary conditions, and §3 briefly considers some aspects of linear theory (including remarks on non-axisymmetry). Sections 4, 5 and 6 give detailed descriptions of the results for various boundary conditions. Section 7 provides such conclusions as are possible given the complexity and detailed nature of the results; some attempt is made to relate these to the Sun although for the most part this task is deferred to a later paper. The text ends with an Appendix on the numerical methods.

2. Basic equations

We consider the motion of incompressible, electrically-conducting fluid in a cylinder of height d and radius r_0 with its axis parallel to the direction of gravity. The velocity and the magnetic field are assumed to be independent of θ where (r, θ, z) are cylindrical polar coordinates. The cylinder has a prescribed quantity of vertical magnetic flux passing through it: in the absence of motion, diffusion ensures that this field is uniform, of strength B_0. To drive convection we impose a temperature difference ΔT between the ends of the cylinder, so that it is heated from below. No heat flux escapes from the curved sidewall.

The equations we need to describe the convection are the Navier–Stokes equation and the induction equation, together with various supplementary relations defining magnetic potential, streamfunction and current (see e.g. Proctor & Weiss 1982). The viscous, thermal, and magnetic diffusivities are ν, κ, and η, respectively. We give the equations in dimensionless form, with d^2/κ as the unit of time, d as the unit of length, B_0 as the unit of magnetic field, and ΔT as the unit of temperature, T. Since the fluid is Boussinesq, and $\nabla \cdot \boldsymbol{B} = 0$, we can let

$$\boldsymbol{u} = \left(-\frac{1}{r}\frac{\partial \psi}{\partial z}, \frac{h}{r}, \frac{1}{r}\frac{\partial \psi}{\partial r}\right), \quad \boldsymbol{B} = \left(-\frac{1}{r}\frac{\partial \chi}{\partial z}, rb, \frac{1}{r}\frac{\partial \chi}{\partial r}\right),$$

where ψ is the streamfunction, h is the specific angular momentum, χ is the poloidal magnetic potential and b is a quantity conserved by axisymmetric motion if there is no diffusion. We write the current as $\boldsymbol{j} = \nabla \times \boldsymbol{B} = (j_r, rJ, j_z)$. The potential vorticity $\Omega = \omega_\theta / r$, where ω_θ is the θ-component of the vorticity, $\nabla \times \boldsymbol{u}$.

Then

$$\Omega = -\nabla \cdot \left(\frac{1}{r^2}\nabla \psi\right), \tag{2.1}$$

and the poloidal part of the velocity distribution is given by

$$\frac{\partial \Omega}{\partial t}+\nabla\cdot(\boldsymbol{u}\Omega)=\nabla\cdot\left(\frac{h^2}{r^4}\hat{\boldsymbol{z}}\right)+\frac{Q\sigma}{q}\nabla\cdot(\boldsymbol{B}\boldsymbol{J}-b^2\hat{\boldsymbol{z}})-R\sigma\nabla\cdot\left(\frac{\hat{\boldsymbol{r}}T}{r}\right)+\sigma\nabla\cdot\left(\frac{1}{r^2}\nabla(r^2\Omega)\right). \quad (2.2)$$

We write the equations in this conservative form for later numerical convenience. Here the Chandrasekhar number, Q, the Rayleigh number, R, the Prandtl number, σ, and the Roberts number q are given by

$$Q=\frac{B_0^2 d^2}{\mu\rho\eta\nu}, \quad R=\frac{g\alpha\Delta T d^3}{\kappa\nu}, \quad \sigma=\frac{\nu}{\kappa}, \quad q=\frac{\kappa}{\eta},$$

μ being the permeability, ρ the density, α the coefficient of expansion and g the local gravity. Note that h is measured in units of κ, so that if h and σ are $O(1)$ the corresponding Ekman number ν/h is $O(1)$: we are not concerned with rapid rotation. The angular momentum is determined by

$$\frac{\partial h}{\partial t}+\nabla\cdot(\boldsymbol{u}h)=\frac{Q\sigma}{q}\nabla\cdot(\boldsymbol{B}r^2 b)+\sigma\nabla\cdot\left[r^2\nabla\left(\frac{h}{r^2}\right)\right]. \quad (2.3)$$

The toroidal field is governed by the θ component of the induction equation,

$$\frac{\partial b}{\partial t}+\nabla\cdot(\boldsymbol{u}b)=\nabla\cdot\left(\boldsymbol{B}\frac{h}{r^2}\right)+\frac{1}{q}\nabla\cdot\left(\frac{1}{r^2}\nabla(r^2 b)\right), \quad (2.4)$$

while the poloidal part is governed by

$$\frac{\partial \chi}{\partial t}+\nabla\cdot(\boldsymbol{u}\chi)=\frac{1}{q}\nabla\cdot\left[r^2\nabla\left(\frac{\chi}{r^2}\right)\right]. \quad (2.5)$$

The final equation we need is the temperature equation,

$$\frac{\partial T}{\partial t}+\nabla\cdot(\boldsymbol{u}T)=\nabla^2 T. \quad (2.6)$$

As we shall see, the choice of boundary conditions is not straightforward: however, we shall assume throughout that the poloidal velocity satisfies stress-free conditions, so

$$\psi=\Omega=0 \quad \text{on } z=0,1 \quad \text{and on } r=A, \quad (2.7)$$

where $A=r_0/d$ is the aspect ratio. We also assume throughout that

$$\frac{\partial \chi}{\partial z}=0 \quad \text{on } z=0,1; \quad \chi=0.5A^2 \quad \text{and} \quad \frac{\partial T}{\partial r}=0 \quad \text{on } r=A. \quad (2.8)$$

Note that $\chi=0.5r^2$ gives a uniform vertical field of strength one in the static state. The cylinder and the boundary conditions specified above are sketched in figure 1. The rectangular section shown there is the domain over which the subsequent contour plots are based.

2.1. *Generation of toroidal field*

We first consider the question of whether the toroidal field in our model has to be imposed, either by having a vertical current flowing through the cell or by imposing a non-zero angular momentum at a boundary, or whether toroidal fields can be

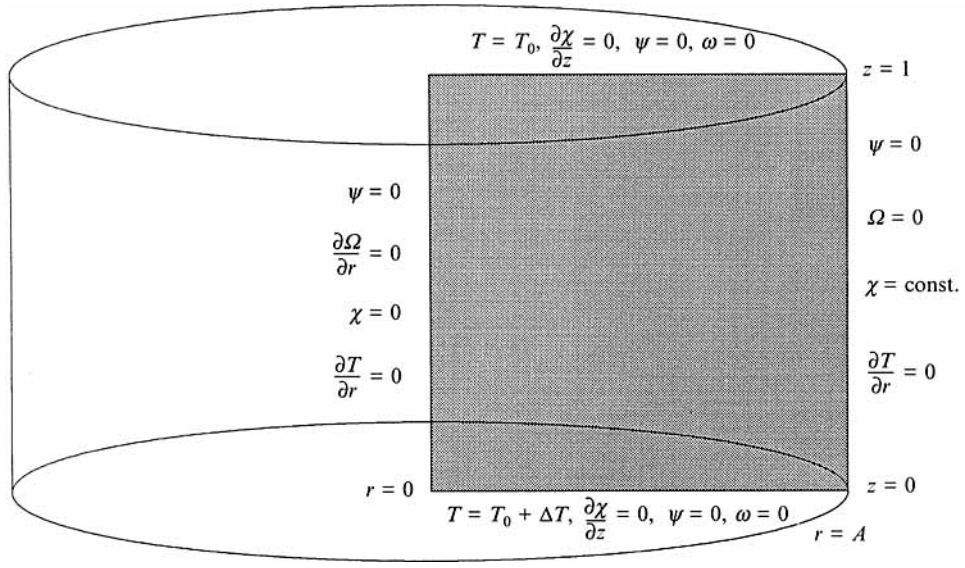

FIGURE 1. The cylinder, with the section used for displaying subsequent contour plots, is shown with the fixed boundary conditions.

generated spontaneously. With a vertical imposed field, motions involving h and b are naturally described as torsional Alfvén waves, so we consider possible driving mechanisms for such waves.

It might seem obvious that an Alfvén wave will decay diffusively since it cannot be driven by buoyancy forces as it involves only toroidal motions. However, if we form the energy equation for the Alfvén waves, by multiplying (2.3) by h/r^2, (2.4) by $Q\sigma br^2/q$, adding, and integrating over the whole cylinder, we obtain

$$\frac{\partial}{\partial t}\int_V \frac{1}{2}\left(\frac{h^2}{r^2}+\frac{Q\sigma b^2 r^2}{q}\right)\mathrm{d}v = \int_V \left(\frac{h^2}{r^4}-\frac{Q\sigma}{q}b^2\right)\frac{\partial \psi}{\partial z}\,\mathrm{d}v - \int_V \sigma r^2 \left|\nabla \frac{h}{r^2}\right|^2 + \frac{Q\sigma}{q^2 r^2}|\nabla b r^2|^2\,\mathrm{d}v \quad (2.9)$$

provided the boundary conditions on h and b are such that

$$\int_S h\nabla\left(\frac{h}{r^2}\right)\cdot \mathrm{d}\boldsymbol{S} = \int_S b\nabla(r^2 b)\cdot \mathrm{d}\boldsymbol{S} = 0 \quad (2.10)$$

on the cylinder surface. From (2.9) we see that even a given fixed velocity field can potentially drive Alfvén waves provided that regions where the radial velocity is inward have large angular momentum and low toroidal field, and regions where the angular velocity is outward have large field and low angular momentum. Nevertheless, we were not able to find any example ψ which drives Alfvén waves. The difficulty appears to be that any significant ψ rearranges the distribution of b and h, sweeping them into boundary layers and hence enhancing the diffusive dissipation. In all solutions examined, this enhanced dissipation wiped out any energy gains from the terms involving ψ in (2.9). We therefore conjecture that Alfvén waves cannot be self-excited with boundary conditions satisfying (2.10).

In consequence, we must examine problems in which either azimuthal field or differential rotation is imposed from the boundaries. There are a number of different ways in which this can be done, but here we consider three different sets of boundary

conditions. In case A we adopt boundary conditions convenient for linear theory, namely

$$\frac{\partial b}{\partial z} = h = 0 \quad \text{on } z = 0, 1; \quad h = 0, \quad b = b_0 \quad \text{on } r = A. \tag{2.11}$$

This latter condition on b is equivalent to specifying the integrated vertical current through the cylinder. Case A is appropriate when the boundary conditions are periodic in z, so that a whole array of convecting cylinders is present. However, for a cylinder in isolation it is of interest to impose the condition that there are no viscous stresses on the cylinder, which gives our case B:

$$\frac{\partial b}{\partial z} = \frac{\partial h}{\partial z} = 0 \quad \text{on } z = 0, 1; \quad \frac{\partial}{\partial r}\left(\frac{h}{r^2}\right) = 0, \quad b = b_0 \quad \text{on } r = A. \tag{2.12}$$

Here we have again imposed the azimuthal field on the $r = A$ boundary; the condition on b at $z = 0, 1$ avoids a radial current sheet developing at the endwalls, although it does permit a non-zero magnetic torque at $z = 0, 1$. Case B is probably the most realistic for a convective cell developing inside a region of twisted magnetic flux.

The third case considered is one where the angular velocity is prescribed at $r = A$, so the azimuthal field is initially absent but is produced by continuously rotating the flux tube. Imposing the condition on b which corresponds to $j_z = 0$ at $r = A$, thus avoiding a vertical current sheet developing there, we get case C:

$$\frac{\partial b}{\partial z} = \frac{\partial h}{\partial z} = 0 \quad \text{on } z = 0, 1; \quad \frac{\partial}{\partial r}(br^2) = 0, \quad h = \omega_0 A^2 \quad \text{on } r = A. \tag{2.13}$$

3. Linear theory

3.1. *Axisymmetric modes*

The equations (2.1)–(2.6) admit solutions of the form $\psi = \Omega = 0$, $T = 0.5 - z$, $\chi = 0.5r^2$, $h = \omega_0 r^2$, $b = b_0$, corresponding to a state of uniform rotation at angular velocity ω_0 with a uniform vertical field and a uniform vertical current of strength $2b_0$. In this section we consider small perturbations to this static solution. If $\omega_0 = b_0 = 0$, the h' and b' fields decouple (primes denote linearized quantities) and we have the magneto-convection problem described by Chandrasekhar (1961; see also Proctor & Weiss 1982). The linearized h and b fields then describe damped torsional Alfvén waves. If $b_0 = 0$ but $\omega_0 \neq 0$, we have rotating magnetoconvection also described by Chandrasekhar (1961): see also Eltayeb (1972, 1975). If $\omega_0 = 0$ and $b_0 \neq 0$, we have the problem of magnetoconvection in a twisted field, which we were unable to find in the literature. However, the stability of the fields without convection has been considered (Roberts 1956; see also Parker 1979). We shall not attempt to discuss the full linear problem $\omega_0 \neq 0$ and $b_0 \neq 0$. Diffusionless instabilities of this type have been studied in the context of magnetic stars in a series of papers by Pitts & Tayler (referenced in Pitts & Tayler 1985).

With $\omega_0 = 0$, and boundary conditions A, (2.11), the spatial dependence of the solution is

$$\psi' \sim \sin(n\pi z)\, rJ_1(kr), \quad \Omega' \sim \sin(n\pi z)\, J_1(kr)/r, \quad \chi' \sim \cos(n\pi z)\, rJ_1(kr),$$
$$b' \sim \cos(n\pi z)\, J_1(kr)/r, \quad h' \sim \sin(n\pi z)\, rJ_1(kr), \quad T' \sim \sin(n\pi z)\, J_0(kr),$$

where the prime denotes the linearized quantity, and non-trivial solutions of $J_1(kA) = 0$ determine k. The non-trivial solution with smallest k is generally the most important. If the first bifurcation is a pitchfork rather than a Hopf bifurcation, it occurs when

$$Rk^2 = a^2(a^4 + n^2\pi^2 Q) - 4n^4\pi^4 Q^2 b_0^2 (a^4 + n^2\pi^2 Q)^{-1}, \tag{3.1}$$

where $a^2 = n^2\pi^2 + k^2$. If $2b_0/a - 1 > a^4/n^2\pi^2 Q$, the instability can set in with negative Rayleigh number: this is the 'sausage' instability of a pinched plasma. The non-axisymmetric version of (3.1) in the diffusionless limit was derived by Roberts (1956). Note that $2b_0 > a$ implies that for aspect ratio 1 and $n = 1$ the 'pitch angle' of the twisted magnetic field (defined as $\tan^{-1}(B_\theta/B_z)$) at the radius $r = A = 1$ is greater than 68°. Since B_θ is proportional to r with uniform current, the critical pitch angle nearer the axis is less than this.

Although in many situations $n = 1$ is the most unstable mode, this is not always true. If b_0 and Q are sufficiently large (which implies the 'sausage' instability is active), instability can occur with lowest negative Rayleigh number with $n > 1$. To find the critical case when $n = 1$ and $n = 2$ onset at the same value of R, we solve (3.1) with $n = 1$ and $n = 2$ simultaneously, which gives rise to a cubic equation for Q. Similarly, we can find the boundary between $n = 2$ and $n = 3$, etc. In figure 2 we plot the critical Q for the mode boundaries as a function of b_0. In the range of b_0 and Q plotted, only the $n = 1$, $n = 2$ and $n = 3$ modes are preferred, but as b_0 is increased, the preferred n also increases.

We can also investigate the condition that transition occurs first at a Hopf bifurcation. It is convenient to proceed by first finding the condition that a Hopf and a pitchfork occur simultaneously (the Takens–Bogdanov bifurcation). This condition is that

$$\sigma(1-q)\tilde{Q}^3\left(1-\frac{4b_0^2}{a^2}\right)+\tilde{Q}^2\left[\sigma(3-2q)+1-\frac{4b_0^2(\sigma(1-2q)-1)}{a^2}\right] + \tilde{Q}[\sigma(3-q)+2]+1+\sigma = 0, \tag{3.2}$$

together with (3.1), where $\tilde{Q} = n^2\pi^2 Q/a^4$. If $b_0 = 0$, (3.2) simplifies to

$$(\tilde{Q}+1)^2\left[\tilde{Q}-\frac{1+\sigma}{\sigma(q-1)}\right] = 0, \tag{3.3}$$

so that in this case a Hopf bifurcation can only occur when there is a positive root for $\tilde{Q}$, i.e. when $q > 1$, and for the Hopf bifurcation to occur first as R is increased, the scaled Chandrasekhar number $\tilde{Q}$ must exceed $(1+\sigma)/\sigma(q-1)$.

When $b_0 \neq 0$ (3.2) must be solved numerically. In figure 3, the contours of Q corresponding to the positive root of (3.2) as a function of q and b_0 are shown, with $\sigma = 1$ and $n = 1$. For the range of parameter space shown there is only one positive root of (3.2) or none. It can be shown by elementary arguments that if $q < 1$ there cannot be more than one positive root. However, if $q > 3$ and $b_0 \approx 2a$ there is a possibility of more than one positive root; in such cases a window of Q may exist where Hopf bifurcation occurs first as R is increased. In figure 3 there are two regions where a Hopf bifurcation can occur first as R is increased; either $q > 1$ and $b_0 < 2a$, as in 'normal' magnetoconvection, or $q < 1$ and $b_0 > 2a$. In either case, the Hopf bifurcation occurs first when Q exceeds the value given in figure 3. For the range of q and b_0 shown in figure 3, the Takens–Bogdanov points occur at negative R if $q < 1$, so here the instability is magnetically driven and the temperature gradient is stabilizing. This is what one expects from the usual argument for overstability in doubly diffusive systems

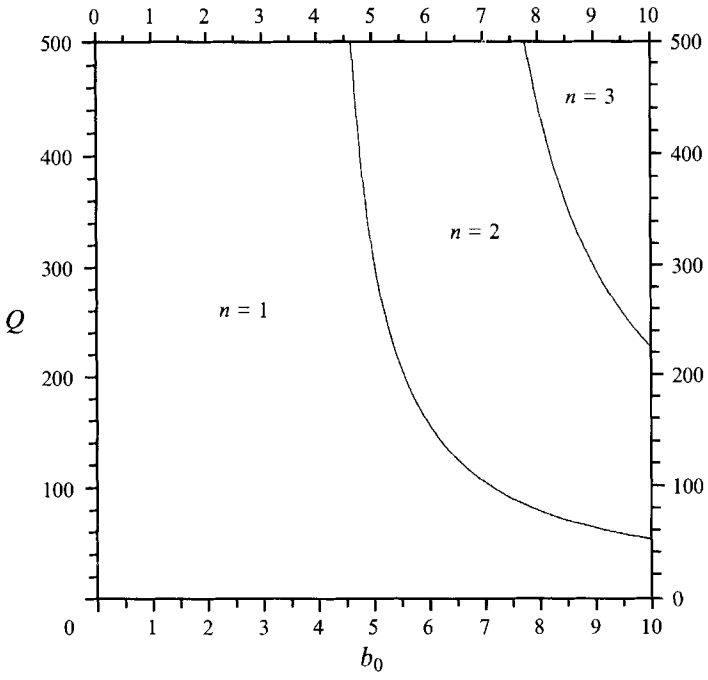

FIGURE 2. The critical Q for the simultaneous onset of modes n and $n+1$ is plotted against b_0. The preferred mode number, n, is also shown.

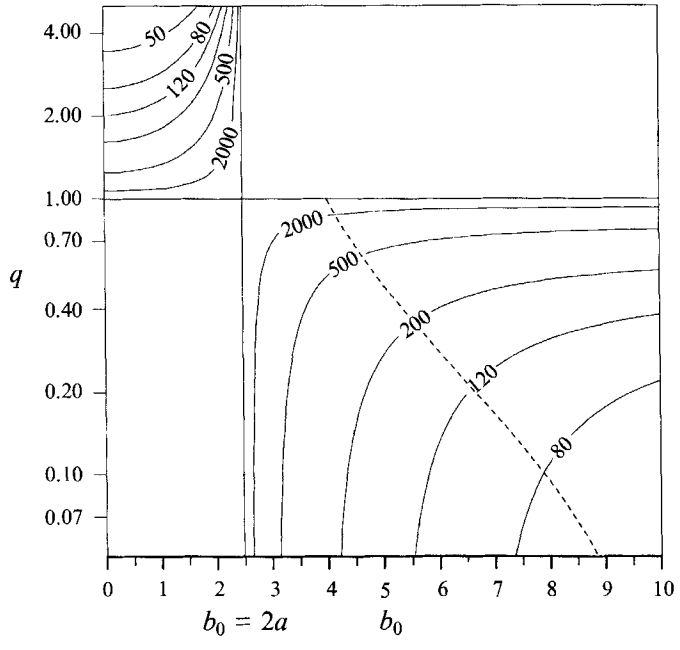

FIGURE 3. Contours of Q for which steady and oscillatory convection onsets simultaneously. Hopf bifurcation occurs first if Q exceeds its critical value. ---, Line of simultaneous onset of the steady $n = 1$ and $n = 2$ modes of convection.

(see e.g. Tritton 1988, p. 386). A parcel of fluid can redistribute its azimuthal field by oscillating in a gravity wave provided the magnetic diffusivity is large relative to the thermal diffusivity, i.e. $q < 1$.

However, it should be noted that if b_0 is moderately large, instability may well onset as a pitchfork with $n = 2$ (or greater) at a lower Rayleigh number than the Hopf with $n = 1$. In figure 3, $n = 2$ is preferred for all points to the right of the dashed curve, so we can only be sure that oscillatory solutions will occur to the left of this dashed curve.

3.2. *Non-axisymmetric modes*

In order to keep the discussion comparatively simple, we shall not in this paper give extensive details on non-axisymmetric instabilities and their nonlinear development. Even with no magnetic field the non-axisymmetric problem is complicated (see e.g. Jones & Moore 1979). We consider only the linear problem where the equilibrium state is non-rotating, and the equilibrium magnetic field is $\boldsymbol{B}_0 = \hat{\boldsymbol{z}} + b_0 r\hat{\boldsymbol{\vartheta}}$. Despite the complexity of the linear equations, it is possible to reduce them to a single equation for the vertical velocity u_z'. This is achieved by taking the z-components of both the curl and the curl–curl of both momentum and induction equations. Elimination of the vertical components of magnetic field, current and vorticity then leaves a twelfth-order system for u_z'. If disturbances are proportional to $\exp(pt)$, this can be written

$$R\sigma\left(p-\frac{1}{q}\nabla^2\right)L^4\nabla_{\mathrm{H}}^2 u_z' = L^8(p-\nabla^2)\nabla^2 u_z' + \frac{4b_0^2 Q\sigma}{q}M^2(p-\nabla^2)\frac{\partial^2 u_z'}{\partial z^2}, \tag{3.4}$$

where
$$M^2 \equiv \frac{Q\sigma}{q}\left(\frac{\partial}{\partial z}+b_0\frac{\partial}{\partial\phi}\right)^2, \quad L^4 \equiv (p-\sigma\nabla^2)\left(p-\frac{1}{q}\sigma\nabla^2\right)-M^2,$$

and ∇_{H}^2 is the horizontal part of ∇^2. This formula can also be used to derive (3.1) and (3.2). A pitchfork bifurcation with $p = 0$ can occur for modes of the form

$$u_z' \sim J_m(kr)\exp \mathrm{i}(m\theta+\lambda z). \tag{3.5}$$

This corresponds to a spiral mode. Unfortunately, such modes are not compatible with a Bénard type problem, where u_z' and T' have to vanish on horizontal surfaces. If the physical boundary conditions (e.g. stress-free impermeable insulating boundaries at $z = 0, 1$ and $r = A$) are imposed, the bifurcation will necessarily be a Hopf bifurcation, and the eigenvalues and eigenfunctions will require numerical solution, which we do not pursue here. Furthermore, if $b_0 \neq 0$ the vertical vorticity is necessarily non-zero, independent of the boundary conditions, which implies that a single solution of the form (3.5) will not satisfy the boundary conditions at $r = A$.

A few elementary observations can be made: if $b_0 = 0$, so there is no twist, m does not appear explicitly in the formula for the Rayleigh number, which is therefore (3.1) with the second term on the right absent. The situation here is similar to that discussed in Jones & Moore (1979). The minimum critical Rayleigh number will depend on m since k is determined by the boundary conditions on the $r = A$ wall, which involve Bessel functions of order m. For some aspect ratios, axisymmetric modes are preferred, for others non-axisymmetric modes, but the linear problem is rather degenerate and nonlinear selection mechanisms are likely to be important.

When Qb_0 is significant, instability can be driven magnetically rather than thermally. The behaviour of periodic modes of type (3.5) may then be more relevant, even though they do not satisfy the prescribed boundary conditions. In this spirit, we can ask which m-values are preferred for the instability of modes (3.5) if we set $R = 0$ in (3.4). If we

increase b_0 at fixed Q, we look for the critical b_0 at which instability occurs. Because modes of the form (3.5) no longer satisfy the boundary conditions, we have to choose λ and k in some reasonable manner. We fix $\lambda = \pi$ so that the modes have the same spatial period as in the cylinder with fixed ends, and also choose $k = \pi$ (on the grounds that as $r \to \infty$ modes of all m asymptote to the same period in the radial direction as they have in the vertical direction). For this problem, at values of $Q < 21.95$ modes with $m = -1$ onset before $m = 0$ modes as b_0 is increased, but for $Q > 21.95$ the axisymmetric mode is the first to become unstable as b_0 is increased.

The above analysis is rather crude, as the choice of λ and k is somewhat arbitrary. However, this critical value of Q is in the dynamically interesting range, and we can perhaps conclude that in some cases non-axisymmetric modes, particularly modes with $|m| = 1$, will be significant in the dynamics, while in other situations, particularly at large Q, axisymmetric modes will predominate. The relative importance of the various modes is also likely to be sensitive to the aspect ratio and boundary conditions imposed at $r = A$ and cannot be resolved without detailed numerical calculations. However, in the rest of the paper we concentrate on the axisymmetric problem.

4. Nonlinear development of the instability

4.1. *Steady solutions*

A finite difference program, based on that developed by Galloway & Moore (1979), was written to follow the nonlinear development of the initial instability. Numerical details are given in the Appendix. The program was started by imposing a small-amplitude initial disturbance of the form $\psi \sim r^2(A-r)\sin \pi z$ to the static solution with $\omega_0 = 0$, $b = b_0$, and evolving the solution in time.

The equations have a symmetry about the midplane, $z = 0.5$. This means that for every solution with fluid rising at the axis, there is a corresponding solution with fluid sinking at the axis:

$$\left.\begin{array}{lll} \psi(r,z) \mapsto -\psi(r,1-z), & \Omega(r,z) \mapsto -\Omega(r,1-z), & \chi(r,z) \mapsto \chi(r,1-z), \\ b(r,z) \mapsto b(r,1-z), & h(r,z) \mapsto -h(r,1-z), & T(r,z) \mapsto -T(r,1-z). \end{array}\right\} \tag{4.1}$$

Which of these two solutions is selected depends on the sign of the initial perturbation. Note that h reverses sign under the transformation while b does not: this is a consequence of boundary conditions A, (2.11). Boundary conditions B behave similarly, but conditions C imply

$$h(r,z) \mapsto h(r,1-z), \quad b(r,z) \mapsto -b(r,1-z).$$

Since the parameter space is rather large, we restricted our attention throughout to $\sigma = 1$ and $A = 1$: these values are assumed henceforth without further comment.

In figure 4 we give an example of a kinematically limited flux rope solution, with $R = 20000$, $Q = 0.1$, $q = 5$, $b_0 = 10$. In all the plots shown in figure 4 (and similar subsequent figures), the axis is on the left-hand side of the box, the right-hand side corresponding to the curved wall (see figure 1). The extreme values of the variable plotted are given in brackets above the relevant plot, and the nine contours are equally spaced at intervals of one-tenth of the difference between these extreme values. Contours corresponding to negative values are shown as dashed, zero contours are shown as dotted, and positive contours are solid. If the extreme values have the same sign (or zero is an extreme), the lowest contour is one-tenth of the difference between the extreme values above the minimum, but if the extreme values are of opposite sign,

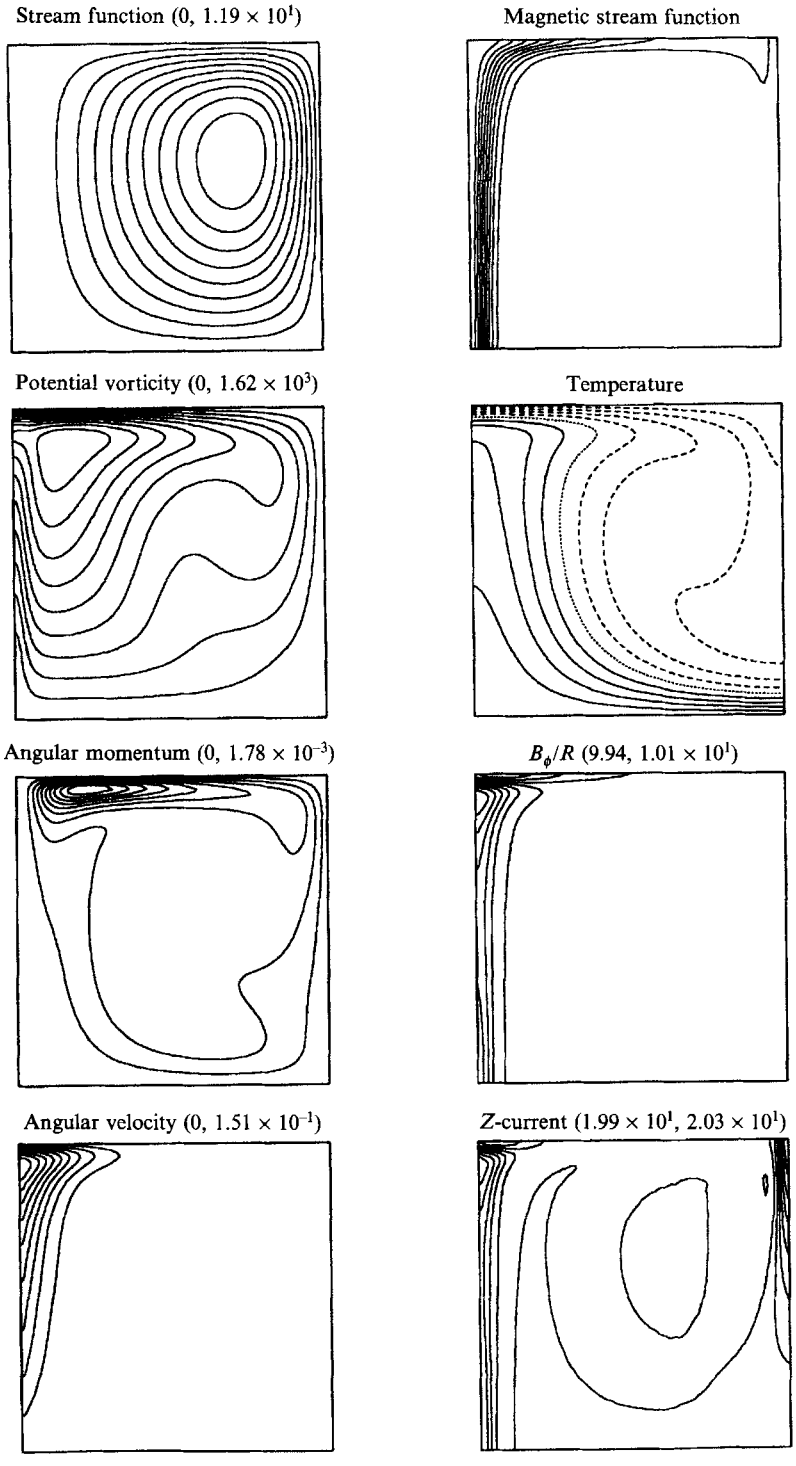

FIGURE 4. Contour plots for the case $R = 20000$, $Q = 0.1$, $q = 5$, $b_0 = 10$, $\sigma = 1$ and $A = 1$, with boundary conditions A.

the contour levels are chosen so that one of the plotted contours is a zero contour. The value of Q in figure 4 is very small, and the Lorentz force plays almost no role in the vorticity equation, and ψ, Ω and T take the values they would achieve in non-magnetic axisymmetric cylindrical convection (Jones, Moore & Weiss 1976). Since the maximum value of the velocity u_z in this solution is around 110, the magnetic Reynolds number R_m defined as $|u_z|_{max} d/\eta$ is $R_m = 550$. The meridional flux is highly concentrated into a rope at the axis, as expected (Galloway *et al.* 1978). In this regime, b is almost constant at b_0 across the cell. Advection and diffusion combine to give b this constant value, set by the boundary condition. The vertical current is also close to its initial uniform value of $2b_0$. The only departures from this state are created by the (small) azimuthal Lorentz force generated primarily by the radial field, since the current is mainly vertical. This generates angular momentum in figure 4, which is concentrated near the top boundary, where the radial field is. The corresponding angular velocity has a maximum on the axis near the top boundary and this stretches out toroidal field, which is why the perturbation to b_0 is concentrated where the angular velocity ω is greatest. The maximum of b occurs close to the maximum of ω but b falls to below b_0 right in the top corner. However, because the Lorentz force is weak, so is h and hence the total range of b at $Q = 0.1$ goes only from 9.944 to 10.009. For small Q this departure from b_0 will scale linearly with Q.

In figure 5, we show the equivalent picture for $R = 20000$, $Q = 100$, $q = 5$, $b_0 = 10$. This is a fairly large Q value, so the flux rope is dynamically limited. With the given initial perturbation, the solution evolves into a steady single-cell solution, despite the fact that the two-cell solution is preferred by linear theory at these parameter values (see figure 2). There is a clear preference for the single-cell solution, because even if the initial disturbance is taken as $\psi \sim r^2(A-r)\sin 2\pi z$, a single-cell solution still results.

As noted by Galloway & Moore (1979), the flux inhibits convection in the rope producing a weak counter-cell and strong negative vorticity, because of the strong shear at the edge of the flux rope. The width of the rope is considerably larger than in the kinematic case. The b distribution is generally similar to that in the kinematic case, but reflects the broadening of b, so that b is also less concentrated. The maximum value of b, 33.4, occurs near the axis at the base of the rope, and b drops off monotonically as we go up the rope to reach a minimum of 3.94 at the top. It is not easy to get very large values of b; if Q is small, the perturbation in b from its mean value of b_0 is highly concentrated, but b itself never varies much from b_0, so no significant amplification of b occurs. On the other hand, if Q is large, the velocities are much reduced by the action of Lorentz force near the rope, and neither the vertical nor the azimuthal field is very strongly concentrated. In the case of figure 5, the peak value of B_z in the rope is approximately 36 (near the bottom of the rope), and the peak value of B_ϕ in the rope (also at the bottom) is approximately 2.8 (recall that $B_\phi = rb$) giving a pitch angle of only about 4°. With $b_0 = 10$, the pitch angle of the initial field rises with r to a value of about 84° at $r = A$. Near the top of the flux rope ($r = 0.1, z = 1$), the vertical field is much less (approximately 10.1), but the azimuthal field is also very weak ($B_\phi \sim 0.37$) and the pitch angle is down to only 2°. We conclude that the effect of the convection is to concentrate the vertical field more than the azimuthal field, so the flux rope is much less twisted than the original unconcentrated field. In essence this comes about because the vertical flux can be kinematically concentrated, whereas the azimuthal flux cannot. Azimuthal flux can only be changed in this model by the action of Lorentz force, but when this is active, narrow flux ropes cannot be produced. This suggests that to produce thin twisted flux tubes, we must appeal to some non-magnetic forcing to produce the azimuthal swirl.

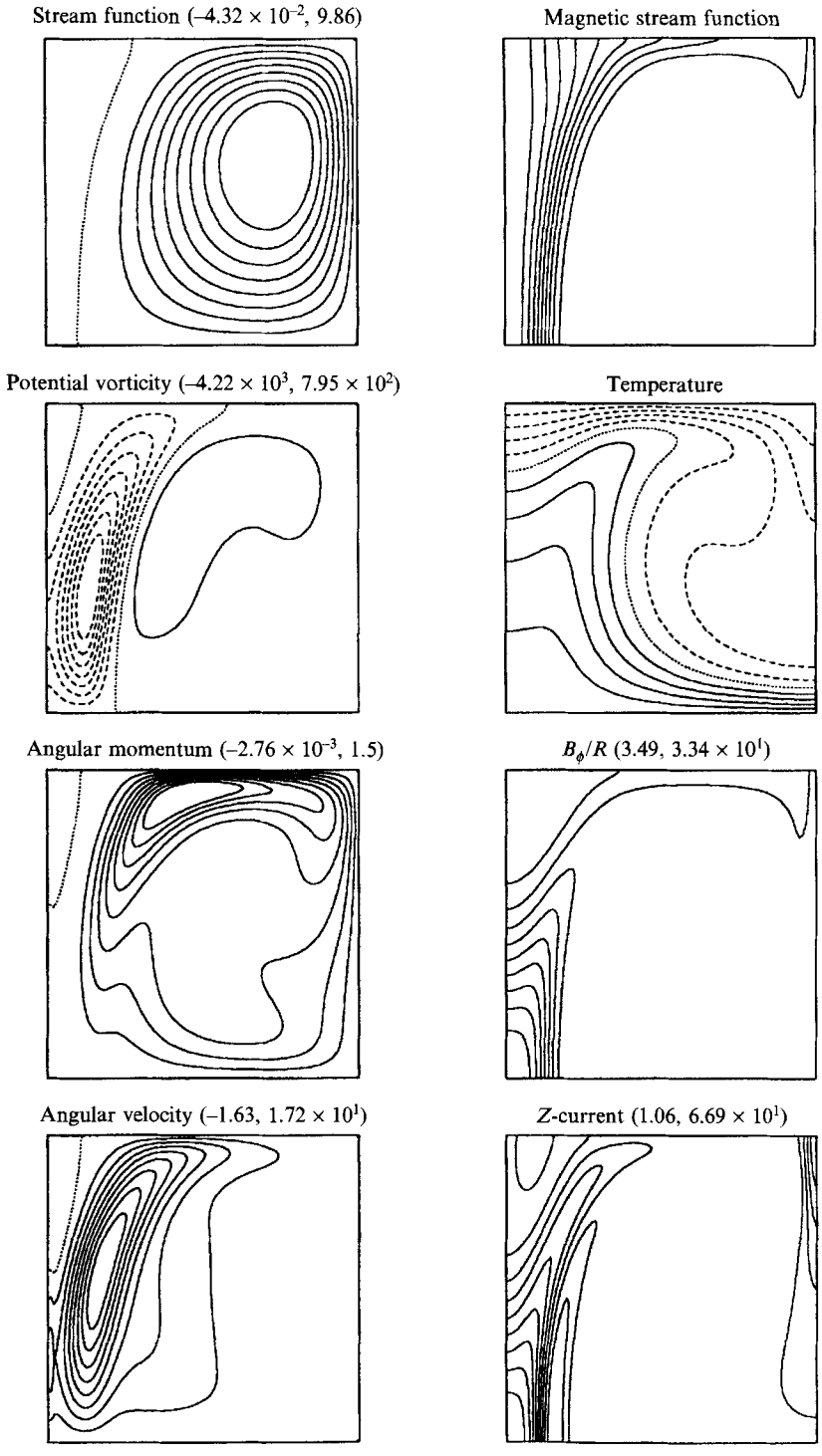

FIGURE 5. Contour plots for the case $R = 20000$, $Q = 100$, $q = 5$, $b_0 = 10$, $\sigma = 1$ and $A = 1$, with boundary conditions A.

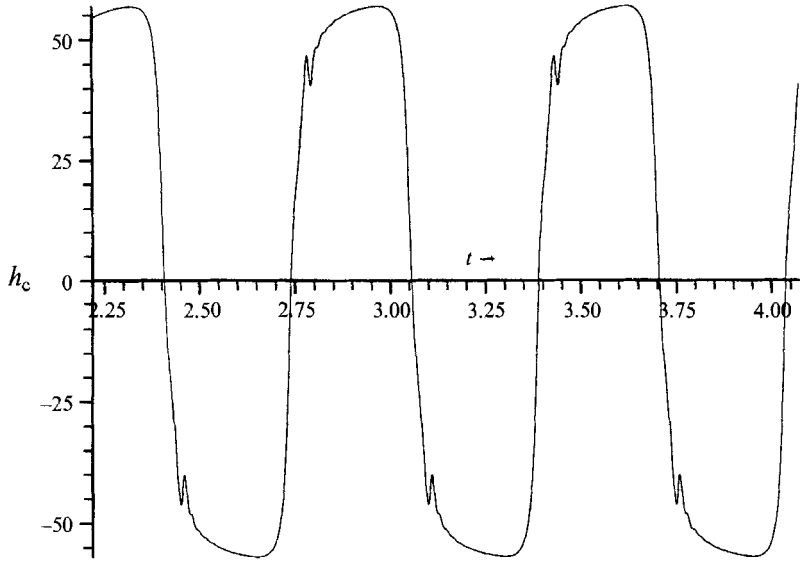

FIGURE 6. The time-dependence of h at the centre of the cell, $r = z = 0.5$, for the case $R = 20000$, $Q = 30$, $q = 0.2$, $b_0 = 20$, $\sigma = 1$ and $A = 1$, with boundary conditions A.

The flux of vertical current through the cylinder ends is fixed by the boundary condition $b = b_0$ at $r = A$. Near the base of the rope, the vertical current has its maximum on the axis, and drops rapidly to below the mean value ($2b_0$) at the edge of the flux rope. The angular momentum distribution is not that dissimilar to the kinematic case, the dominant contribution coming from the interaction of the vertical current with the radial field splayed out at the top of the cell. However, because the flux rope is much less concentrated in the dynamical case, the angular momentum, and particularly the angular velocity, is larger lower down the flux rope. The corresponding angular velocity is, however, more concentrated near the outside edge of the flux rope.

The azimuthal field can, in principle, affect the vorticity through the terms $\partial b^2/\partial z$ and $\partial h^2/\partial z$, but changing b_0 from 0 to 10 hardly changes the vorticity distribution at all, so the dynamical effect of the azimuthal field is slight compared to the effect of the poloidal field in these flux rope solutions.

4.2. *Oscillatory solutions*

If q is small, so that magnetic diffusion is large and the magnetic Reynolds number is moderate, a concentrated flux rope does not develop. At small Q steady solutions occur, but as Q is increased, periodic oscillations occur. This is actually rather surprising; although the linear theory of §3 shows that a Hopf bifurcation can occur at small q, it also suggests that oscillations can occur only at negative Rayleigh number, whereas we are finding oscillations at positive Rayleigh number. The basic linear physical mechanism is that gravity waves are rendered unstable by the pinch effect coming from magnetic flux diffusing into the fluid. This cannot operate at positive Rayleigh number, as gravity waves can only exist in a stably stratified medium. The mechanism must therefore be a nonlinear one, a view confirmed by our numerical experiments.

In figure 6, we show the angular momentum at the centre of the cell as a function of time, for the case $R = 20000$, $Q = 30$, $q = 0.2$, $b_0 = 20$. The shape of the graph suggests that the system is flipping between two states, and this is confirmed by contour

(*a*)

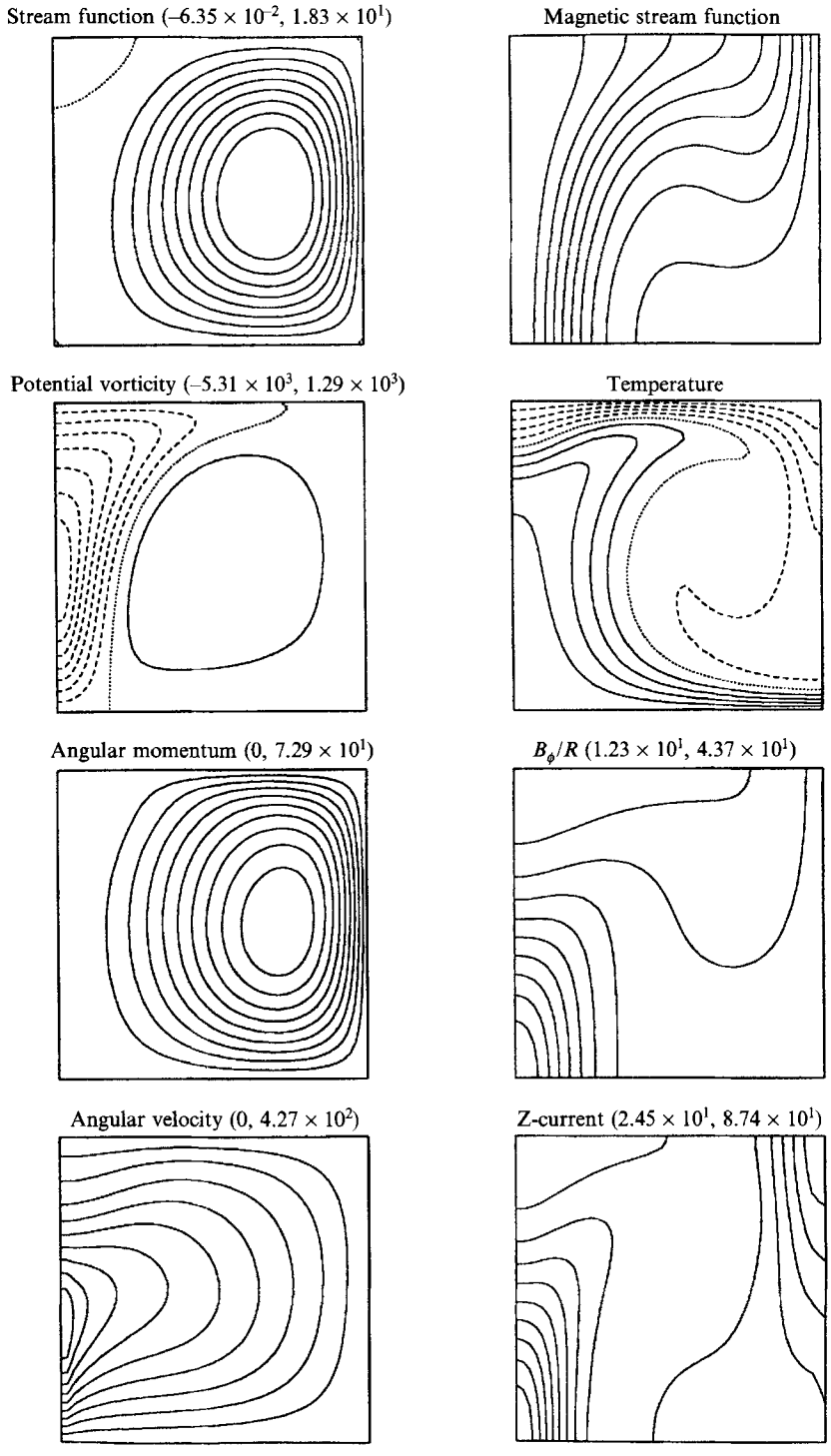

FIGURE 7(*a*). For caption see p. 313.

(*b*)

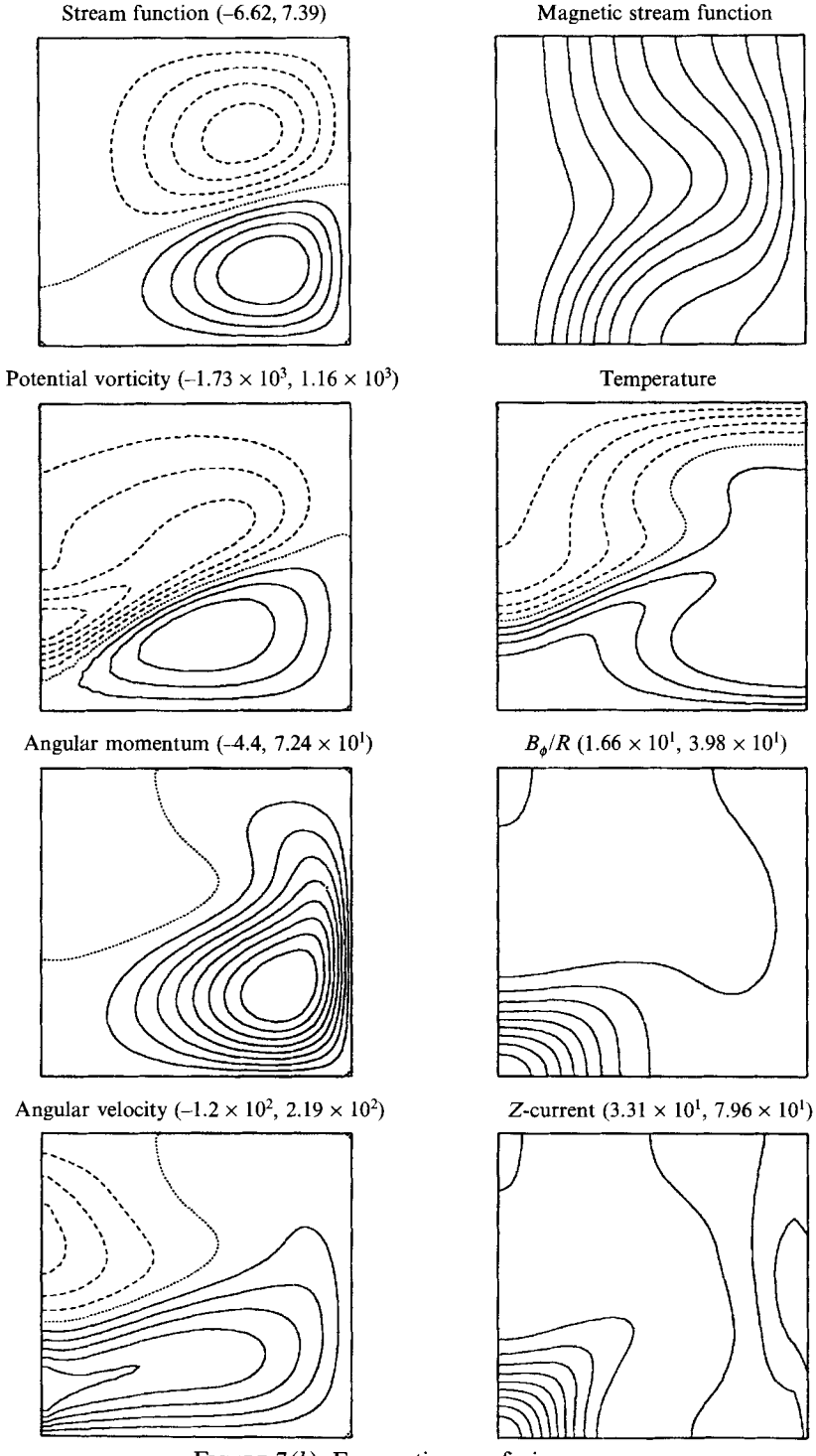

FIGURE 7(*b*). For caption see facing page.

(*c*)

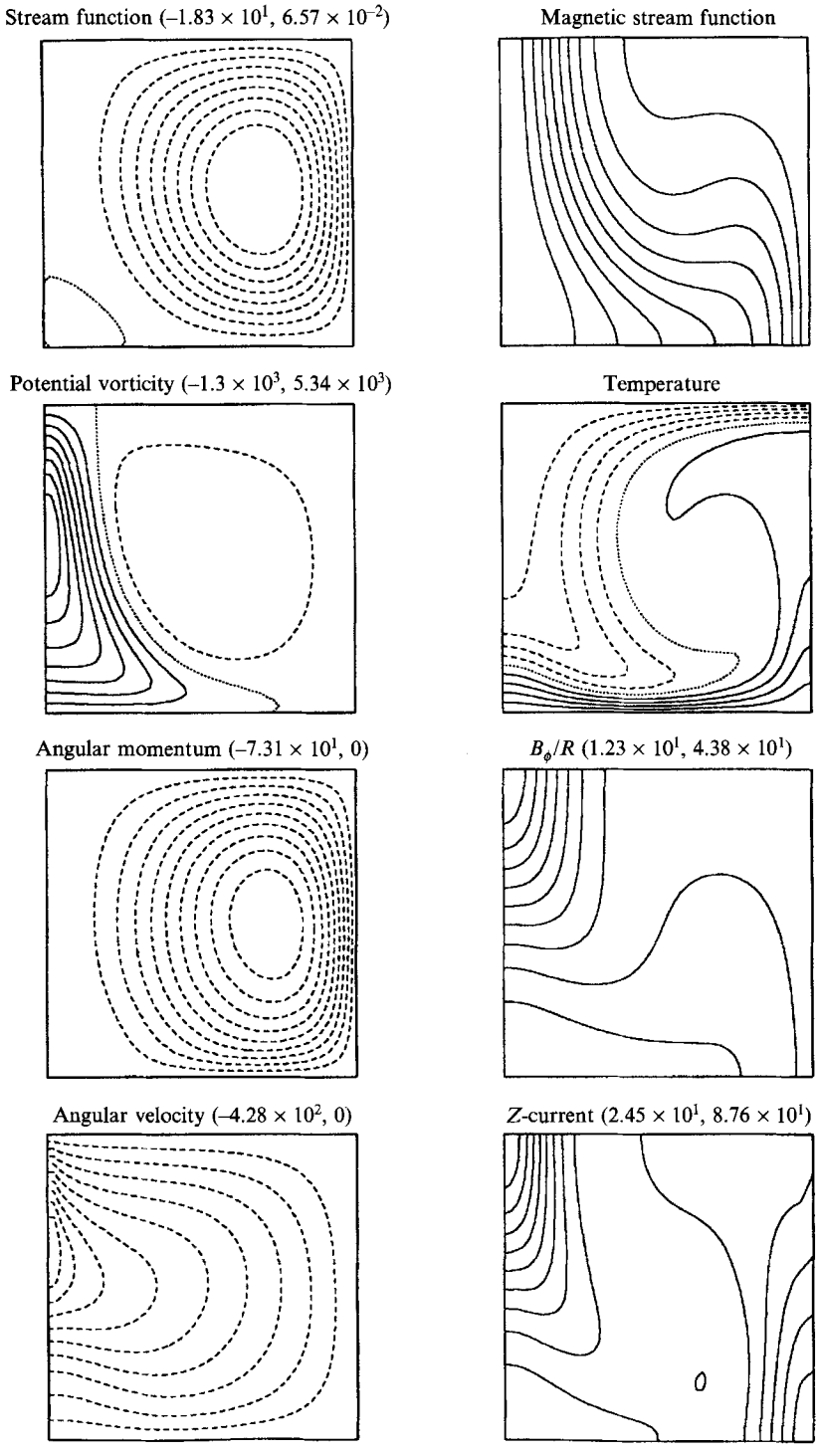

FIGURE 7. Contours plots at three different times during the oscillation shown in figure 6, (*a*) time $t = 2.22$; (*b*) time $t = 2.41$; (*c*) time $t = 2.54$.

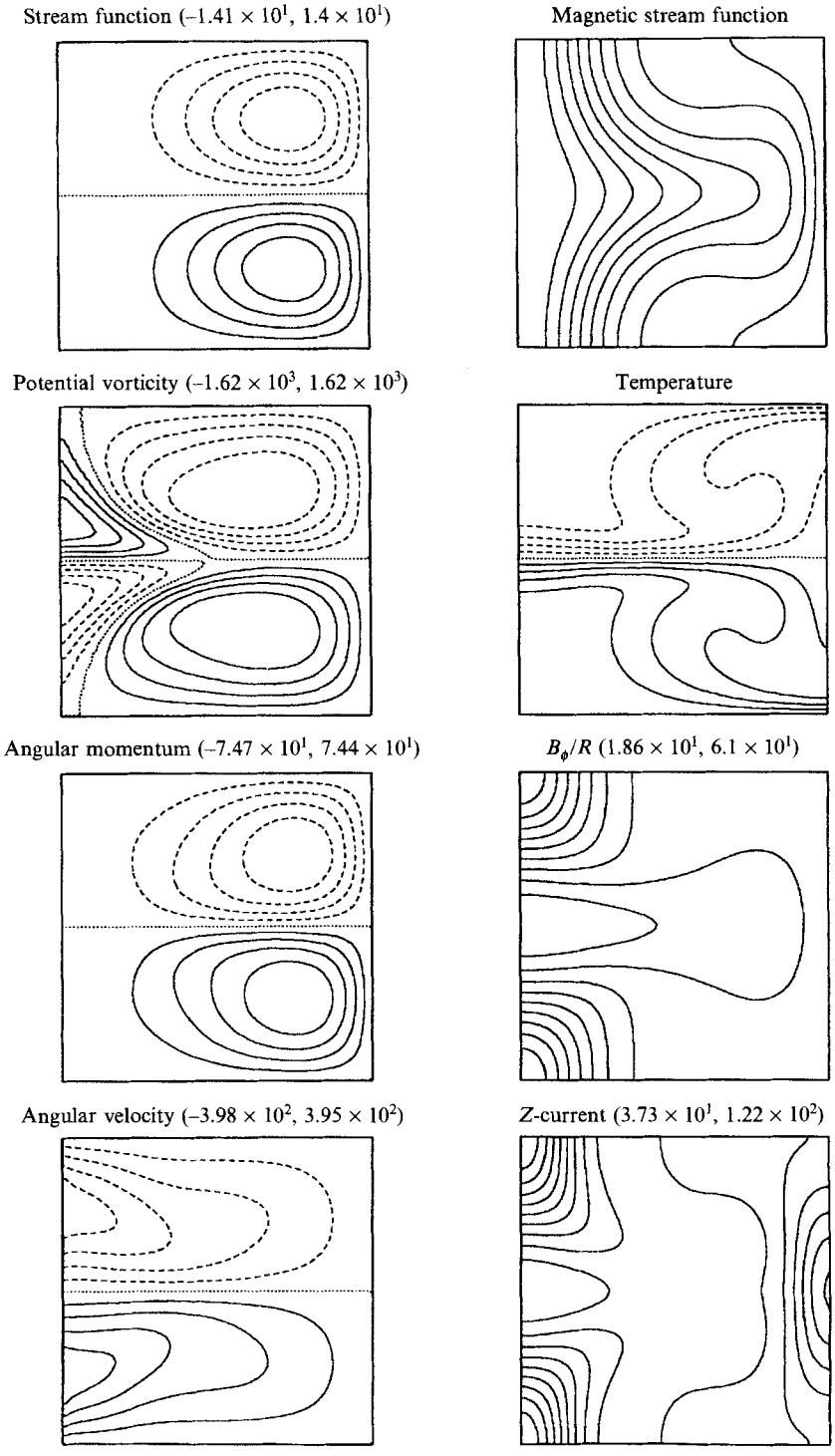

FIGURE 8. Contour plots for the case $R = 20000$, $Q = 30$, $q = 0.2$, $b_0 = 30$, $\sigma = 1$ and $A = 1$, with boundary conditions A. At this value of b_0, a two-cell solution is preferred.

plots at three different times: in figure 7 we see the nature of the solutions at the times $t = 2.22$, 2.41 and 2.54. In figure 7(*a*) the solution corresponds to a single cell with fluid rising at the axis; this can be inferred from the temperature and magnetic stream function plots. The circulation is essentially in one direction except for a small counter-cell near the axis at the top. The angular momentum is all of one sign, and b has a maximum on the axis near the bottom of the cell. As time proceeds, the small counter cell grows, and is roughly equal in size with the original cell in figure 7(*b*). This phase of two cells of equal strength lasts only briefly, and is followed by a state typified by figure 7(*c*) which has fluid sinking at the axis. This is essentially the opposite parity to figure 7(*a*) under transformation (4.1). The oscillation consists, therefore, of periodic oscillation between two states of opposite parity. If the value of b_0 is reduced, the period of the oscillation increases: at $b_0 = 22$, the period is 0.492: at $b_0 = 20$ it is 0.693, whereas at $b_0 = 18$ it has increased right up to 1.574. We conjecture that the solution approaches a heteroclinic orbit as b_0 is reduced below 18. At the heteroclinic point, the symmetrical pair of steady solutions must lose their stability to a perturbation which connects the two solutions. The full bifurcation diagram associated with this behaviour is currently under further investigation. The behaviour is probably connected with instability to a double-cell solution; if we increase b_0 the oscillatory branch eventually jumps to a steady double-cell solution of the type shown in figure 8, which is for $b_0 = 30$. The preference for a two-cell solution as b_0 is increased is predicted by linear theory (figure 2). This preference is overruled at large q by the nonlinear formation of flux ropes, but at small q the magnetic field solutions resemble linear solutions, and breakup into smaller cells can occur.

5. Stress-free boundary conditions

The boundary conditions adopted in §4 were those appropriate to a periodic configuration in z. We now consider what differences occur if we adopt boundary conditions B, that is (2.12). These conditions differ from the periodic ones only in the stress-free boundary conditions imposed on the angular momentum. Since stress-free conditions have been imposed on the meridional flow, this is a more realistic condition for an isolated convective cell occurring in a region of twisted magnetic field.

In figure 9 we show the solution for $R = 20000$, $Q = 100$, $q = 5$ and $b_0 = 10$, the same parameter values as for figure 5. Comparing these two figures, we see that ψ, Ω, χ and T are very little changed. This reflects the fact noted earlier, that the Lorentz and centrifugal forces associated with b and h, respectively, are not very significant, so changes in b and h do not feed back into the other fields. However, the plots of h and b in figure 9 are significantly different from those of figure 5. The most remarkable change is that near the axis the sign of b is reversed. The effect of the convection has been to twist the flux rope in the opposite direction from the way the initial field is twisted. The angular momentum distribution is affected directly by the change in boundary conditions but h is still all of one sign in figure 9; the angular velocity distributions are not so very different, having a maximum at the edge of the flux rope, but which in figure 9 occurs below the figure 5 maximum.

The explanation of the reversal of b comes from conservation of angular momentum. If we integrate (2.3) over the volume of the cylinder, we obtain

$$\frac{\partial}{\partial t}\int_V h\,\mathrm{d}v = -\int_S \boldsymbol{u}h\cdot\mathrm{d}\boldsymbol{S} + \frac{Q\sigma}{q}\int_S \boldsymbol{B}r^2 b\cdot\mathrm{d}\boldsymbol{S} + \sigma\int_S r^2\nabla\left(\frac{h}{r^2}\right)\cdot\mathrm{d}\boldsymbol{S}. \tag{5.1}$$

Now $\boldsymbol{u}\cdot\mathrm{d}\boldsymbol{S}$ will always be zero, since the mass is contained in the cylinder. With

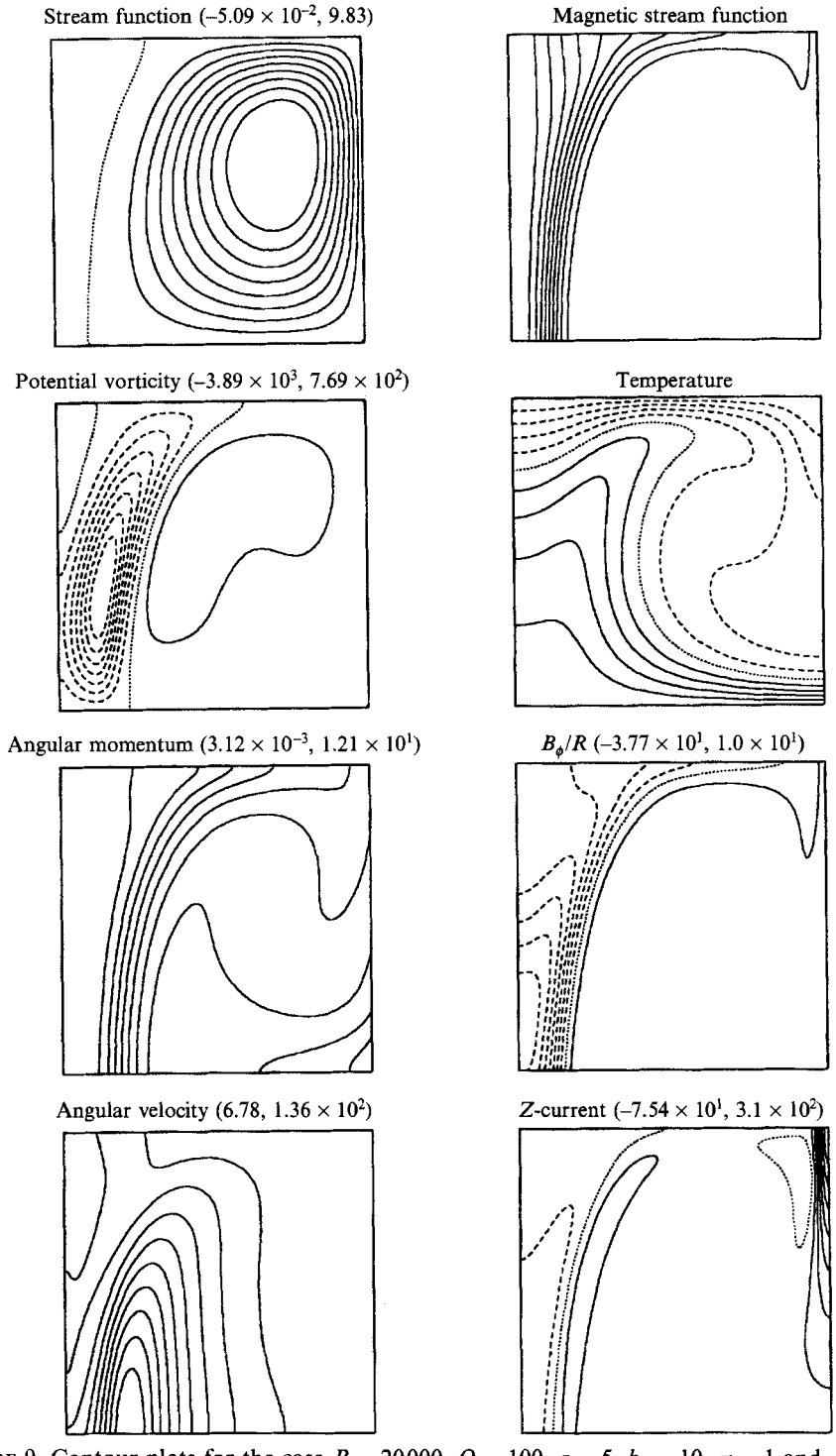

FIGURE 9. Contour plots for the case $R = 20000$, $Q = 100$, $q = 5$, $b_0 = 10$, $\sigma = 1$ and $A = 1$, with boundary conditions B. Note the appearance of reversed sign b.

stress-free boundary conditions, the third integral will also vanish, as there can be no viscous torques acting on the cylinder from outside. The Lorentz torque must therefore vanish in a steady state so

$$\int_S \boldsymbol{B} r^2 b \cdot \mathrm{d}\boldsymbol{S} = 0. \tag{5.2}$$

Now, there is no contribution from the curved surface since there is no radial B there. The integral over the bottom surface must be very small unless b is enormous there: this is because B_z is concentrated into a rope near the axis, so B_z is small outside the rope, and the term is weighted with r^2. Such a large b would lead to a Lorentz force in the meridional direction which could not be balanced, so we conclude that the bottom boundary cannot produce much Lorentz torque. The contribution from the top surface must therefore be small also. Since b is prescribed as b_0 at $r = A$, and B_z is comparatively uniform over the top surface, the integrand cannot be uniformly small: it can only achieve a small overall value by cancellation of positive and negative fractions. So b has to have a sign change over the top surface, and hence over the whole cell. If we apply the same argument to the figure 5 case, it is still true that the Lorentz torque coming from the bottom and the side is small, but now the large term coming from the top is balanced by a large viscous stress: note the large angular momentum gradient at the top of the cell in figure 5.

We now examine the degree to which the field is twisted backwards. Near the bottom of the cell, $-b$ reaches its maximum, but $-B_\phi$ is larger near the top. In consequence, the maximum reverse pitch angle is only about 6° at the bottom, but is approximately 64° at the top, attained at $r \sim 0.35$. This is almost as much as the forward pitch angle of the initial state at this radius.

Some runs were also performed with boundary conditions B at small q. Oscillatory solutions of a similar nature were found in much the same region of parameter space as for conditions A, suggesting that the occurrence of the periodic solutions is quite robust.

6. Azimuthal field created by imposed external flow

6.1. *Steady solutions*

We also considered the problem where no fixed aximuthal field is specified, but azimuthal field is created by differential rotation within the convecting cell. We assume here that this imposed azimuthal flow is created by some external agency, such as the influence of rotation on large-scale convection in the solar convection zone, for example. We model this by assuming that the angular momentum at $r = A$ has a specified value $h_0 = \omega_0 A^2$. We do not then need a non-zero b_0 to produce azimuthal field, so b_0 is set to zero. This corresponds to boundary conditions C (2.13).

This type of forcing can generate narrow, twisted flux ropes because we no longer rely on the Lorentz force to produce enhanced azimuthal field. At small Q and large magnetic Reynolds number we get a thin flux rope, and, provided the angular velocity near the rope is of the same order as that imposed at the edge of the cell, a strong azimuthal field is produced.

In figure 10 we show the case $R = 50000$, $Q = 1$, $q = 1$, and $h_0 = 10$. As this value of Q is quite modest, the flux is strongly concentrated into a rope. Comparing the stream function, potential vorticity, temperature and magnetic stream function plots with those of figure 4, we see they are quite similar, so the value of Q is low enough for them to be unaffected by Lorentz forces, the only exception being the negative

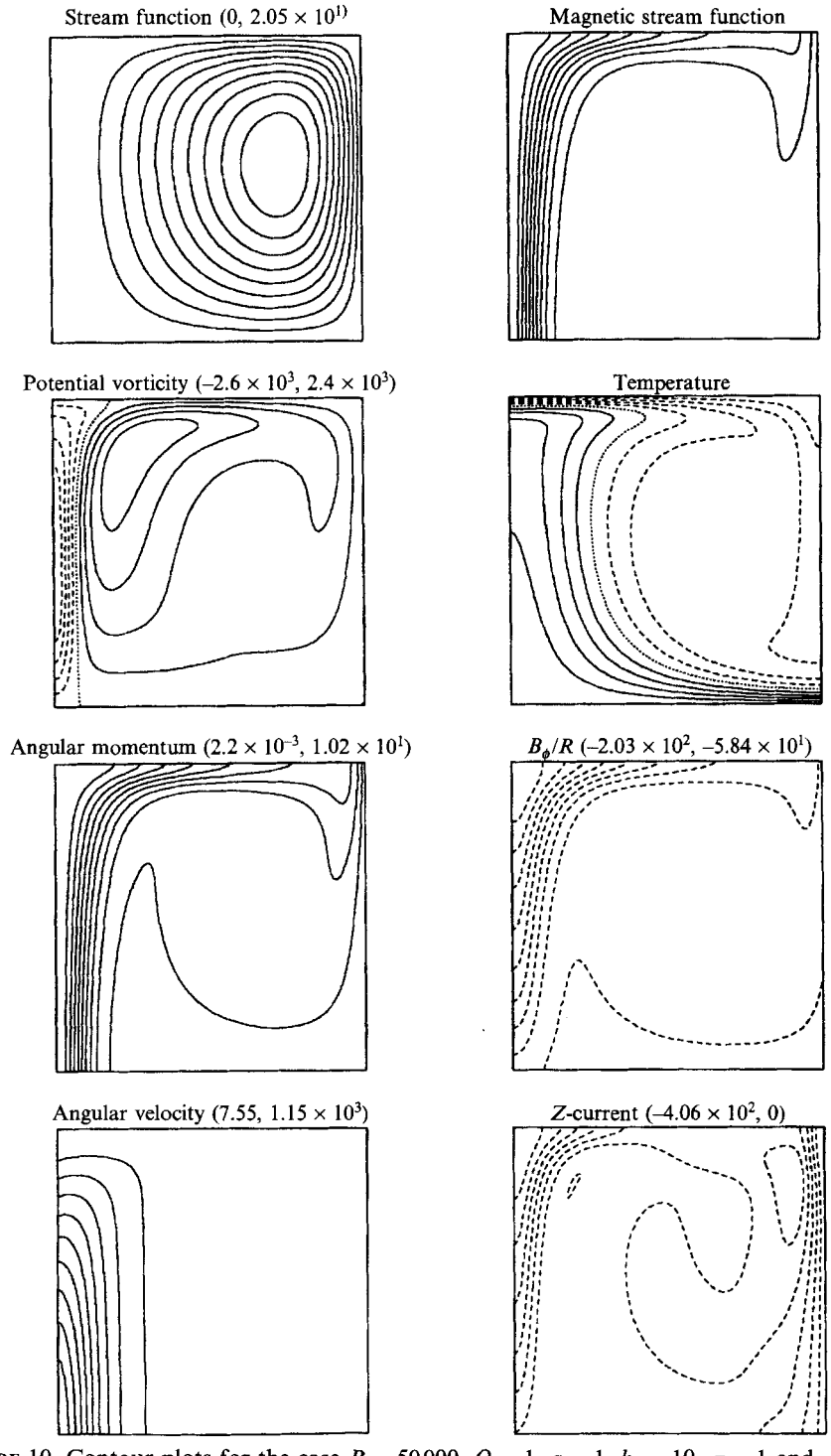

FIGURE 10. Contour plots for the case $R = 50000$, $Q = 1$, $q = 1$, $h_0 = 10$, $\sigma = 1$ and $A = 1$, with boundary conditions C.

potential vorticity near the axis. This is due to two effects: the Lorentz force near the axis is not quite negligible, because the large local value of the vertical field strength enhances its effect. Even if Q is made much smaller, there is still some negative vorticity near the axis produced by the angular momentum distribution: this can be eliminated by reducing h_0.

The big difference between this case of external rotation forcing and forcing by an imposed vertical current is in the size and distribution of the azimuthal field and velocity. The value of Q is sufficiently small for the angular momentum not to be significantly affected by the Lorentz force; also the value of h_0 is sufficiently small for there to be little influence of the angular momentum on the potential vorticity except near the axis. The distribution of angular momentum is therefore governed by advection and diffusion from the velocity field determined by the convection. Not surprisingly, therefore, the angular momentum plot in figure 10 resembles the magnetic stream function plot, which is governed by the same processes.

The angular momentum distribution gives rise to an angular velocity distribution which has a strong maximum near the axis, and is largest at the bottom. It is here that conservation of angular momentum leads to strong spin-up (Galloway 1978), the 'spinning ice-skater' phenomenon. The distribution of b drawn out by the ω-effect can be predicted from the magnetic stream function plots and the angular velocity. b is all negative, the largest value occurring on the axis near the top of the rope. $\partial\omega/\partial z$ is negative here stretching out vertical field, and this is reinforced by negative $\partial\omega/\partial r$ stretching out the radial component of field. Note that the strength of b is much larger than that occurring in figure 5.

The different distribution of b produced by an imposed external flow means that the field is strongly twisted near the top of the cell with a pitch angle near 90°. In this case the strongest azimuthal field occurs at the top of the cell where the vertical field is comparatively weak: the degree of twist is much smaller near the bottom of the flux rope where B_z is stronger and B_ϕ is weaker.

In figure 11 we show the case $R = 50000$, $Q = 30$, $q = 1$ and $h_0 = 10$. The larger value of Q means that Lorentz forces have come into play. Their effect on the axial flow is predictable: the broadening of the flux rope, and the reverse flow near the axis being clearly visible. The most striking change, however, is the angular momentum reversal at the top of the cell. This reverse flow is produced by the Lorentz force: if a path along the axial field lines near the top of the cell is followed, b varies only slowly but r^2b becomes more negative. The term $(\boldsymbol{B}\cdot\nabla)br^2$ is therefore negative, and hence provides the negative torque required. One might expect that an argument such as that used in §5 to explain the reversal of b could be used. If we integrate (2.4) over the cylinder, we obtain

$$\frac{\partial}{\partial t}\int_V b\,\mathrm{d}v = -\int_S \boldsymbol{u}b\cdot\mathrm{d}\boldsymbol{S} + \int_S \frac{\boldsymbol{B}h}{r^2}\cdot\mathrm{d}\boldsymbol{S} + \int_S \frac{1}{r^2}\nabla(br^2)\cdot\mathrm{d}\boldsymbol{S}. \tag{6.1}$$

The first integral on the right-hand side vanishes, since there is no flow across the boundaries, and the contributions to the third integral at the curved surface and the top and bottom boundaries vanish because of the boundary conditions imposed on b. However, there is a non-zero contribution from the third integral at the axis: if we consider a cylinder of radius ϵ and then let $\epsilon \to 0$ we see there is dissipation of toroidal field at the axis. In consequence, the second integral is not necessarily zero.

The distribution of b has also been significantly changed by the Lorentz force. The maximum negative value is no longer at the top of the cell but is on the axis about halfway up. The magnitude of b is also reduced by the Lorentz force, but this is not

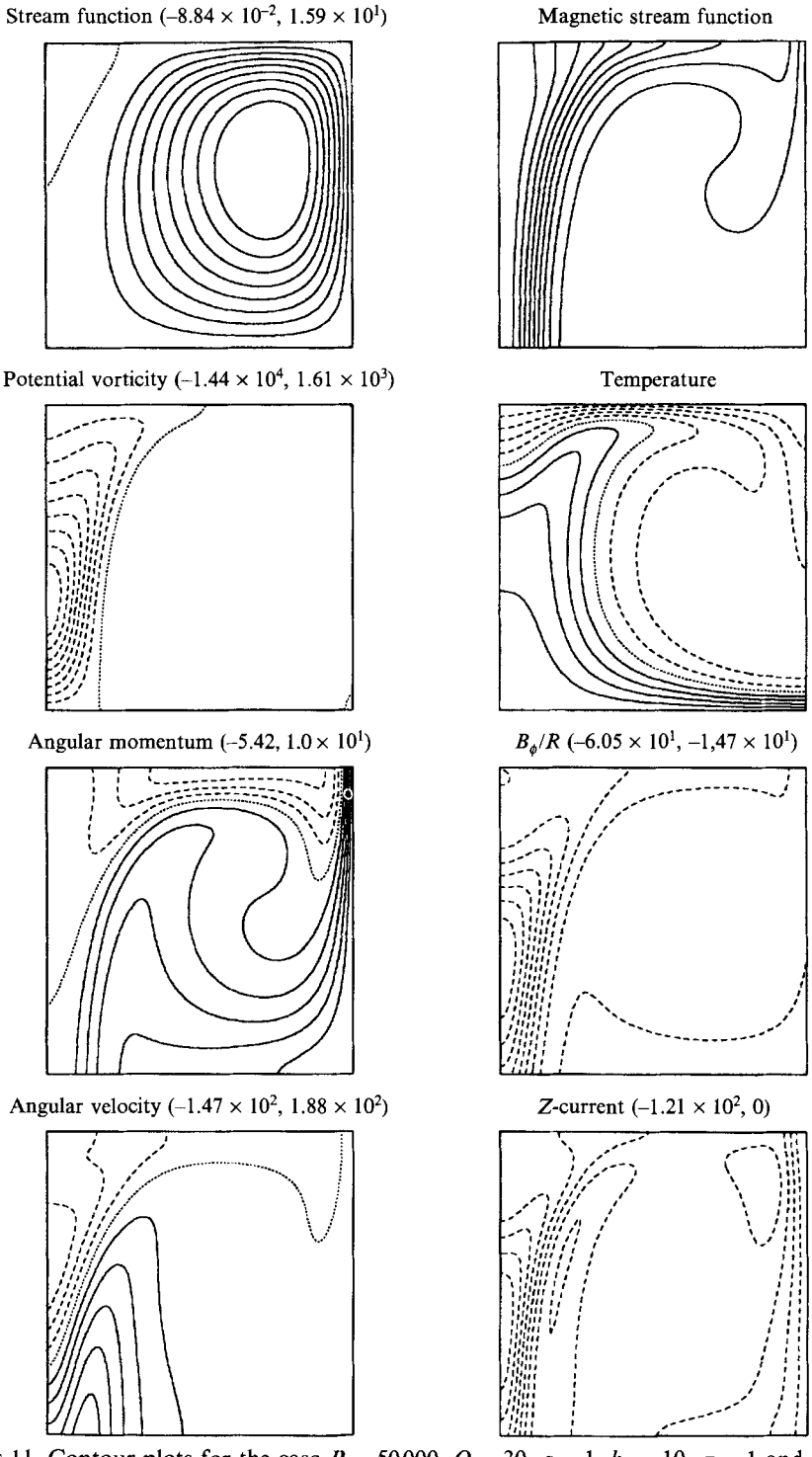

FIGURE 11. Contour plots for the case $R = 50000$, $Q = 30$, $q = 1$, $h_0 = 10$, $\sigma = 1$ and $A = 1$, with boundary conditions C. Note the appearance of reversed sign h.

surprising as the angular velocity gradient is much reduced because of the broadening of the magnetic flux rope.

6.2. *Oscillatory solutions*

Oscillatory behaviour generally resembling that found in §4 was also found in this case. It was found at small Q, so Lorentz force is not important, at large q (the opposite limit from the §4 case) and at $h_0 \sim 15$. Clearly, the dynamical effect required to produce oscillations is supplied by the term $\partial h^2/\partial z$ in the equation of motion (2.2). The period of the oscillation is long (about 5.0 in units of the thermal diffusion time at $h_0 = 14$) and the form of the oscillation is a continual flipping between states with fluid rising and then falling at the axis, similar to figures 7(*a*) and 7(*c*). However, the transition between these states involves two cells in the radial direction rather than two cells in the vertical. So the effect of the angular momentum is evidently to exert a preference for tall thin cells rather than short fat ones. Apart from this distinction, the phenomenon appears similar to the small q oscillations, and probably arises from a heteroclinic orbit.

7. Conclusions

We first summarize the answer to the question of whether strongly twisted ropes of magnetic flux can be formed by convection. A simple but important feature is that advection by a meridional flow does not expel the azimuthal field produced by a uniform axial current, it leaves it unchanged. If acting on a non-uniform current, advection will tend to produce uniformity, but this does not produce a current rope. In this respect, the vertical current behaves quite differently from the vertical field, which is concentrated into a rope by advection provided the magnetic Reynolds number is large.

In order to produce a concentrated current, we must rely on differential rotation to twist the vertical flux rope produced by advection of meridional flux. It is at this point that the difference between the two methods of imposing azimuthal flux has a big effect.

If the azimuthal flux is maintained by a fixed vertical current through the cell, as with boundary conditions A and B, differential rotation can only be produced by the action of Lorentz force. This, in effect, rules out the possibility of strongly twisted flux ropes developing. If the Chandrasekhar number Q is small, Lorentz forces are weak, very little azimuthal motion is driven, and so very little ω-effect occurs to generate new B_ϕ. On the other hand, if the Chandrasekhar number is large, Lorentz forces act on the meridional flow and prevent the formation of a concentrated flux rope. In this case, a significant differential rotation can develop, but it has no concentrated vertical flux to work on. We conclude that whatever the value of Q, it is not possible to produce concentrated flux ropes with $O(1)$ twist using a fixed vertical current through the cell.

If the azimuthal field is maintained by rotational driving, keeping the outer edge rotating at fixed velocity while the cell convects, strongly twisted ropes can be formed. In this case we do not require the Lorentz force to generate the ω-effect, as this is produced by the redistribution of angular momentum by the convection. At small Q this differential rotation can act directly on the concentrated vertical flux to produce concentrated azimuthal flux. This is the mechanism envisaged by Childress (1979). We may summarize the distinction between the two cases by noting that for concentrated twisted flux ropes we need a flux of vertical vorticity through the cell; a flux of vertical current density is not sufficient. In any case, this is the mechanism we have in mind for the situation in the Sun, and it appears to be effective; convection can intensify vorticity and hence generate field-aligned currents.

The next conclusion, which we found quite surprising, is that with stress-free boundary conditions convection can actually produce negative sign azimuthal flux, when only positive flux is imposed. There is an analogous result in the case of imposed positive rotation, where regions of negative u_ϕ occur, although the details of the mechanisms involved may be rather different in the two cases.

In the case of negative flux production, one would expect that the Lorentz force would produce a differential rotation that would generate azimuthal field opposed to any initially present: this is, after all, how a torsional Alfvén wave is formed. The surprise is that in the steady state this effect is strong enough to produce a negative azimuthal field with a larger magnitude than the imposed positive field. As we saw in §5, the phenomenon can be explained in terms of the need for the total external torque produced by the Lorentz force on the whole cell to vanish.

The reason for negative angular velocity production is still not entirely clear to us, in the sense that we have no simple argument which shows when negative angular velocity must occur. What is clear is that the effect can only be produced by Lorentz force: advection and diffusion of angular momentum on their own can never produce negative angular momentum. As we saw in §6, the negative angular momentum produced in figure 11 is consistent with the Lorentz force pattern, but we cannot say how general the phenomenon is. From our numerical experience, we believe that angular momentum reversal occurs in a wide range of parameter space.

The third point of interest is the existence of oscillatory solutions in a much wider variety of circumstances than linear theory would indicate. Indeed, in this twisted flux problem, linear theory is an even feebler guide to what actually occurs than is the case in purely axial magnetoconvection. In that problem, Galloway & Moore (1979) found that time-dependent behaviour occurred more or less where expected from linear theory, but the form and periods of the time-dependence were poorly determined by linear considerations. Here we find time-dependence where none is predicted by linear theory. The form of the oscillation, and the fact that periodic branches terminate in heteroclinic orbits, indicate that these are nonlinear oscillations. They appear to be associated with changes in the convection pattern, where the preferred number of rolls in the box is changing between one and two. A similar phenomenon has recently been found in spherical α^2-dynamo models by Hollerbach (1991). This suggests that the phenomenon is rather general, and amenable to explanation in terms of amplitude equations. Physically, such oscillations can only occur when there is a significant input from either h or b into the equation of motion for the axial flow. This requires either Lorentz force to be significant (i.e. non-negligible Q) or the vertical angular momentum gradients to be significant. The presence of either can give rise to these long-period oscillations.

In this paper we have concentrated on the more mathematical aspects of the problem. A difficulty is the large number of non-dimensional parameters, coupled with the variety of the boundary conditions that can be applied. It is impractical to conduct a systematic search; our procedure has instead been to isolate certain physical ideas and pick those parameters and boundary conditions that seem best for examining them. There are undoubtedly other kinds of possible behaviour yet to be discovered. Regarding applications, it seems twisting convective motions could generate field-aligned currents on the Sun. Although our model is Boussinesq, there is no reason why this mechanism would not work equally well in a fully compressible fluid, providing the degree of evacuation of the flux tube is not extreme. The way these currents return is very dependent on the boundary conditions, but for our case C (probably the most appropriate for the Sun of those treated), most of the current passes through the cell

in or around the axial flux rope, with a lesser contribution at the outer wall. This gives little information on the return path, but suggests the cell tries to pass the currents up into the atmosphere. In our figures 10 and 11, the currents are all of one sign. Applying Ampère's law shows that B_ϕ must be fairly substantial throughout the cell; in our geometry there is no way around this if the currents do not return with opposite sign. As stressed above, such fields are transported passively, without significant effect on the driving convection. This effect would have observable consequences; currents of order 10^{12} A are thought to be generated by twists (Melrose 1991), and the associated horizontal B_ϕ would be around 10^{-2} T, i.e. 100 G, say 10000 km away from the fluxrope. This ought to be detectable; correspondingly, its absence would tell us that the currents are returning somehow without our seeing them. We did a few runs with $b = 0$ at $r = A$, thus forcing no net current to pass through the top and bottom boundaries; in those cases, the returning z-current occurred mainly in a sheath surrounding the fluxrope.

To assess what this means for the solar atmosphere, it is necessary to add a model for the upper regions, specifying how the magnetic field lines return to the photosphere. This is a very difficult problem, though some progress has been made in considering the reaction to twisting of the atmosphere alone, both analytically (Zweibel & Boozer 1985; Lothian & Hood 1989; Browning 1990) and numerically (Steinolfson 1989).

D.J.G. is grateful for support from an SERC visiting fellowship, Grant no. GR/G41580.

Appendix. Numerical methods

Numerical solutions to equations (2.1)–(2.8) were found using a code based on the conservative finite-difference approach described in Roberts & Weiss (1966), and in Moore, Peckover & Weiss (1974). The code is an extension of that described in Galloway & Moore (1979), and is based on a version developed in collaboration with Moore for use in cylindrical shell geometry. This version solves the evolution equation for χ in its conservative form (2.5), rather than in the non-conservative form used in Galloway & Moore (1979); a similar equation (2.3) is solved for the evolution of h. Because our computational domain includes the axis, we had to modify the scheme locally to cope with the coordinate singularity there. This required a variety of devices, of which a representative selection will be given presently.

Away from the axis, the procedure adopted is straightforward. We will describe it here for equation (2.3); the others are treated analogously. The quantity $h^n_{j,k}$ is regarded as the average over the annular region $(j-1)\Delta r < r < (j+1)\Delta r$, $(k-1)\Delta z < z < (k+1)\Delta z$, and the divergence terms are evaluated as fluxes out of the same annulus, or, in the case of the diffusive terms, as fluxes out of the annulus $(j-\frac{1}{2})\Delta r < r < (j+\frac{1}{2})\Delta r$, $(k-\frac{1}{2})\Delta z < z < (k+\frac{1}{2})\Delta z$ suitably scaled up by the ratio of volumes, which is 4. Here $\Delta r = \Delta z = \Delta$ is the mesh size, and n refers to the timestep. The mesh sizes and the diffusive maximum for the timestep are set up at the beginning of the run and the timestep is reset occasionally as demanded by the Courant condition, incorporating the various velocities and Alfvén speeds. Advective fluxes are conserved across the large annuli and diffusive fluxes across the small ones. Note that away from the axis, the same equations result when the quantities are regarded as averages over the small annuli, with the advective fluxes scaled down accordingly. This is not true at the axis.

As in the earlier references, a leapfrog scheme is used on a pair of staggered meshes, with a Dufort–Frankel form for the diffusion term. Writing out the terms according to the above philosophy, the difference equation form of (2.3) becomes

$$\left(\frac{h_{j,k}^{n+1}-h_{j,k}^{n}}{\Delta t}\right)2\pi r_j\,2\Delta r\,2\Delta z = \text{Adv.}+\text{Lor.}+\text{Visc.}$$

where

$$\text{Adv.} = \left(\frac{\psi_{j+1,k+1}^{n+\frac{1}{2}}-\psi_{j+1,k-1}^{n+\frac{1}{2}}}{r_{j+1}\,2\Delta z}\right)h_{j+1,k}^{n+\frac{1}{2}}\,4\pi r_{j+1}\,\Delta z+\left(\frac{\psi_{j-1,k+1}^{n+\frac{1}{2}}-\psi_{j-1,k-1}^{n+\frac{1}{2}}}{r_{j-1}\,2\Delta z}\right)h_{j-1,k}^{n+\frac{1}{2}}\,4\pi r_{j-1}\,\Delta z$$
$$+\left(\frac{\psi_{j+1,k+1}^{n+\frac{1}{2}}-\psi_{j-1,k+1}^{n+\frac{1}{2}}}{r_j\,2\Delta r}\right)h_{j,k+1}^{n+\frac{1}{2}}\,2\pi r_j\,2\Delta r-\left(\frac{\psi_{j+1,k-1}^{n+\frac{1}{2}}-\psi_{j-1,k-1}^{n+\frac{1}{2}}}{r_j\,2\Delta r}\right)h_{j,k-1}^{n+\frac{1}{2}}\,2\pi r_j\,2\Delta r,$$

$$\text{Lor.} = \frac{Q\sigma}{q}\left[\left(\frac{\chi_{j+1,k+1}^{n+\frac{1}{2}}-\chi_{j+1,k-1}^{n+\frac{1}{2}}}{r_{j+1}\,2\Delta z}\right)r_{j+1,k}^{2}\,b_{j+1,k}^{n+\frac{1}{2}}\,4\pi r_{j+1}\,\Delta z\right.$$
$$-\left(\frac{\chi_{j-1,k+1}^{n+\frac{1}{2}}-\chi_{j-1,k-1}^{n+\frac{1}{2}}}{r_{j-1}\,2\Delta z}\right)r_{j-1,k}^{2}\,b_{j-1,k}^{n+\frac{1}{2}}\,2\pi r_{j-1}\,2\Delta z$$
$$\left.-\left(\frac{\chi_{j+1,k+1}^{n+\frac{1}{2}}-\chi_{j-1,k+1}^{n+\frac{1}{2}}}{r_j\,2\Delta r}\right)r_j^2\,b_{j,k+1}^{n+\frac{1}{2}}\,4\pi r_j\Delta r+\left(\frac{\chi_{j+1,k-1}^{n+\frac{1}{2}}-\chi_{j-1,k-1}^{n+\frac{1}{2}}}{r_j\,2\Delta r}\right)r_j^2\,b_{j,k-1}^{n+\frac{1}{2}}\,4\pi r_j\,\Delta r\right],$$

$$\text{Visc.} = 4\sigma\left[2\pi r_{j+\frac{1}{2}}\Delta z r_{j+\frac{1}{2}}^{2}\left(\frac{h_{j+1,k}^{n+\frac{1}{2}}}{r_{j+1}^{2}\Delta r}-\frac{h_{j,k}^{n+1}+h_{j,k}^{n}}{2r_j^2\,\Delta r}\right)\right.$$
$$\left.-2\pi r_{j-\frac{1}{2}}\Delta z r_{j-\frac{1}{2}}^{2}\left(-\frac{h_{j-1,k}^{n+\frac{1}{2}}}{r_{j-1}^{2}\Delta r}+\frac{h_{j,k}^{n+1}+h_{j,k}^{n}}{2r_j^2\,\Delta r}\right)+2\pi r_j\,\Delta r r_j^2\left(\frac{h_{j,k+1}^{n+\frac{1}{2}}+h_{j,k-1}^{n+\frac{1}{2}}-(h_{j,k}^{n+1}+h_{j,k}^{n})}{r_j^2\,\Delta z}\right)\right].$$

This can be rearranged to give an explicit expression to update $h_{j,k}^{n}$ to $h_{j,k}^{m+1}$ using variables on the alternate mesh (as in the earlier work, ψ and χ must be interpolated):

$$h_{j,k}^{n+1} = h_{j,k}^{n}+\frac{j\Delta t}{4j^2(\Delta)^3+\sigma\Delta t\,\Delta(8j^2+3)}$$
$$\times\left\{-(\psi_{j+1,k+1}^{n+\frac{1}{2}}-\psi_{j+1,k-1}^{n+\frac{1}{2}})\,h_{j+1,k}^{n+\frac{1}{2}}+(\psi_{j-1,k+1}^{n+\frac{1}{2}}-\psi_{j-1,k-1}^{n+\frac{1}{2}})\,h_{j-1,k}^{n+\frac{1}{2}}\right.$$
$$+(\psi_{j+1,k+1}^{n+\frac{1}{2}}-\psi_{j-1,k+1}^{n+\frac{1}{2}})\,h_{j,k+1}^{n+\frac{1}{2}}-(\psi_{j+1,k-1}^{n+\frac{1}{2}}-\psi_{j-1,k-1}^{n+\frac{1}{2}})\,h_{j,k-1}^{n+\frac{1}{2}}$$
$$+\frac{Q\sigma}{q}[(\chi_{j+1,k+1}^{n+\frac{1}{2}}-\chi_{j+1,k-1}^{n+\frac{1}{2}})\,r_{j+1,k}^{2}\,b_{j+1,k}^{n+\frac{1}{2}}-(\chi_{j-1,k+1}^{n+\frac{1}{2}}-\chi_{j-1,k-1}^{n+\frac{1}{2}})\,r_{j-1,k}^{2}\,b_{j-1,k}^{n+\frac{1}{2}}$$
$$-(\chi_{j+1,k+1}^{n+\frac{1}{2}}-\chi_{j-1,k+1}^{n+\frac{1}{2}})\,r_j^2\,b_{j,k+1}^{n+\frac{1}{2}}+(\chi_{j+1,k-1}^{n+\frac{1}{2}}-\chi_{j-1,k-1}^{n+\frac{1}{2}})\,r_j^2\,b_{j,k-1}^{n+\frac{1}{2}}]$$
$$+4\sigma j\Delta\left[h_{j,k+1}^{n+\frac{1}{2}}+h_{j,k-1}^{n+\frac{1}{2}}+\frac{(j+\frac{1}{2})^3}{j(j+1)^2}h_{j+1,k}^{n+\frac{1}{2}}+\frac{(j-\frac{1}{2})^3}{j(j-1)^2}h_{j-1,k}^{n+\frac{1}{2}}\right.$$
$$\left.\left.-\left(2+\frac{(j+\frac{1}{2})^3+(j-\frac{1}{2})^3}{j^3}\right)h_{j,k}^{n}\right]\right\}.$$

The above equation fails for the mesh point one out from the axis. The apparent singularity has no physical basis and is removed when we take into account the form $h = h_2(z,t)\,r^2+\ldots$ taken by h near the axis. Using this analytical form, we integrate over the cylinder $0<r<\Delta r$, $(k-1)\,\Delta z<z<(k+1)\,\Delta z$ to get an expression for the rate of

change of h_2 due to the advective flux terms in (2.3). We integrate over the smaller cylinder $0 < r < \frac{1}{2}\Delta r$, $(k-\frac{1}{2})\Delta z < z < (k+\frac{1}{2})\Delta z$ to get the rate of change due to the diffusive flux terms. Then we add the results to get the total rate of change of h_2. Writing $H = (\Delta r)^2 h_2$ gives, after some manipulation, the difference equation

$$H_{0,k}^{n+1} = H_{0,k}^{n} + \frac{\Delta t}{\Delta^3 + 5\sigma\Delta\Delta t}\Big(2(\psi_{1,k+1}^{n+\frac{1}{2}} - \psi_{1,k-1}^{n+\frac{1}{2}})\, h_{1,k}^{n+\frac{1}{2}} + \psi_{1,k-1}^{n+\frac{1}{2}} H_{0,k-1}^{n+\frac{1}{2}} - \psi_{1,k+1}^{n+\frac{1}{2}} H_{0,k+1}^{n+\frac{1}{2}}$$

$$+ \frac{Q\sigma}{q}\Delta^2[\chi_{1,k+1}^{n+\frac{1}{2}} b_{0,k+1}^{n+\frac{1}{2}} - \chi_{1,k-1}^{n+\frac{1}{2}} b_{0,k-1}^{n+\frac{1}{2}} + 2(\chi_{1,k-1}^{n+\frac{1}{2}} - \chi_{1,k+1}^{n+\frac{1}{2}})\, b_{1,k}^{n+\frac{1}{2}}]$$

$$+ \sigma\Delta[H_{0,k+1}^{n+\frac{1}{2}} + H_{0,k-1}^{n+\frac{1}{2}} + 8h_{1,k}^{n+\frac{1}{2}} - 10H_{0,k}^{n}]\Big),$$

where subscript 0 denotes the axis and subscript 1 the meshpoint one out. The asymptotic forms for the other variables as $r \to 0$ are that ψ and χ go like r^2 whilst Ω, b, T and J go like functions of z + terms of order r^2. Some of these forms have been exploited in deriving the above formula; note too that the vertical velocity (resp. magnetic field) on the axis is $2/(\Delta r)^2$ times ψ (resp. χ) one mesh point out (cf. Galloway & Moore 1979). The conservation properties of the scheme must be sacrificed here; h has one definition in terms of the average over the large cylinder (for advective fluxes and forces), and another based on the average over the small cylinder (for diffusive fluxes). As stated above, these can be combined sensibly only away from the axis. The scheme adopted here has the advantage that it reduces to the appropriate form when either advection or diffusion operates in isolation.

Once H is known, an equation to update h one meshpoint out can be derived along similar lines. In fact, virtually all the equations (and interpolation formulae) need special treatment at the axis and one meshpoint out. The details are too extensive to give here, but the general approach was as for the equation for H given above. For instance, we derived an equation to update the value of Ω on the axis. Even though it is correct to second order to set the value there equal to the value two meshpoints out (Jones *et al.* 1976, appendix), in practice it is inaccurate because all quantities change rapidly near the axis.

REFERENCES

BROWNING, P. K. 1990 Twisted flux loops in the solar corona. *Geophysical Monographs 58: Physics of Magnetic Flux Ropes* (ed. C. T. Russell, E. R. Priest & L. C. Lee), pp. 219–228. American Geophysical Union.

CHANDRASEKHAR, S. 1961 *Hydrodynamic and Hydromagnetic Stability*. Oxford University Press.

CHILDRESS, S. 1979 A class of solutions of the magnetohydrodynamic dynamo problem. In *The Application of Modern Physics to the Earth and Planetary Interiors* (ed. S. K. Runcorn), pp. 629–648. Wiley.

CHILDRESS, S. & SOWARD, A. M. 1985 On the rapid generation of magnetic fields. In *Chaos in Astrophysics*, NATO Advanced Research Workshop, Palm Coast, Florida, USA (ed. J. R. Buchler, J. M. Perdang & E. A. Spiegel), pp. 223–244. Reidel.

ELTAYEB, I. A. 1972 Hydromagnetic convection in a rapidly rotating fluid layer. *Proc. R. Soc. Lond.* A **326**, 229–254.

ELTAYEB, I. A. 1975 Overstable hydromagnetic convection in a rapidly rotating fluid layer. *J. Fluid Mech.* **71**, 161–179.

GALLOWAY, D. J. 1978 Convection with a magnetic field or rotation: an analogy. In *Proceedings of the Workshop on Solar Rotation*, Catania Astrophysical Observatory (ed. G. Belvedere & L. Paternó), pp. 352–357.

GALLOWAY, D. J. & MOORE, D. R. 1979 Axisymmetric convection in the presence of a magnetic field. *Geophys. Astrophys. Fluid Dyn.* **12**, 73–105.

GALLOWAY, D. J., PROCTOR, M. R. E. & WEISS, N. O. 1978 Magnetic flux ropes and convection. *J. Fluid Mech.* **87**, 243–261.

HOLLERBACH, R. 1991 Parity coupling in α^2-dynamos. *Geophys. Astrophys. Fluid Dyn.* **60**, 245–260.

HUGHES, D. W. & PROCTOR, M. R. E. 1988 Magnetic fields in the solar convection zone: magnetoconvection and magnetic buoyancy. *Ann. Rev. Fluid Mech.* **20**, 187–223.

JONES, C. A. & GALLOWAY, D. J. 1993 Alpha-quenching in cylindrical magnetoconvection. *Proc. NATO ASI conf. Theory of Solar and Planetary Dynamos, Cambridge 1992* (to appear).

JONES, C. A. & MOORE, D. R. 1979 Stability of axisymmetric convection. *Geophys. Astrophys. Fluid Dyn.* **14**, 61–101.

JONES, C. A., MOORE, D. R. & WEISS, N. O. 1976 Axisymmetric convection in a cylinder. *J. Fluid Mech.* **73**, 353–388.

LOTHIAN, R. & HOOD, A. W. 1989 Twisted magnetic flux tubes: the effects of small twist. *Solar Phys.* **122**, 227–244.

MELROSE, D. B. 1991 Neutralised and unneutralised current patterns in the solar corona. *Astrophys. J.* **381**, 306–312.

MOORE, D. R., PECKOVER, R. S. & WEISS, N. O. 1974 Difference methods for time-dependent two-dimensional convection. *Comput. Phys. Commun.* **6**, 198–220.

NORDLUND, Å., BRANDENBURG, A., JENNINGS, R. L., RIEUTORD, M., RUOKOLAINEN, J., STEIN, R. F. & TUOMINEN, I. 1992 Dynamo action in stratified convection with overshoot. *Astrophys. J.* **392**, 647–652.

PARKER, E. N. 1979 *Cosmical Magnetic Fields, their Origin and their Activity*. Clarendon.

PITTS, E. & TAYLER, R. J. 1985 The adiabatic stability of stars containing magnetic fields. 6. The influence of rotation. *Mon. Not. R. Astr. Soc.* **216**, 139–154.

PRIEST, E. R. 1982 *Solar Magnetohydrodynamics*. Dordrecht: D. Reidel.

PROCTOR, M. R. E. & WEISS, N. O. 1982 Magnetoconvection. *Rep. Prog. Mod. Phys.* **45**, 1317–1379.

ROBERTS, P. H. 1956 Twisted magnetic fields. *Astrophys. J.* **124**, 430–442.

ROBERTS, K. V. & WEISS, N. O. 1966 Convective difference schemes. *Maths Comput.* **20**, 272–299.

SOWARD, A. M. & CHILDRESS, S. 1986 Analytic theory of dynamos. *Adv. Space Res.* **8**, 7–18.

STEINOLFSON, R. S. 1990 Dynamics of axisymmetric loops. *Geophysical Monographs 58: Physics of Magnetic Flux Ropes* (ed. C. T. Russell, E. R. Priest & L. C. Lee), pp. 211–218. American Geophysical Union.

TRITTON, D. J. 1988 *Physical Fluid Dynamics*. Clarendon.

ZWEIBEL, E. G. & BOOZER, A. H. 1985 Evolution of twisted magnetic fields. *Astrophys. J.* **295**, 642–647.